Universidad Carlos III de Madrid

NUMERICAL STUDY OF A ONE STAGE GAS GUN

Universidad Carlos III de Madrid

Alfredo Escalante López

Tutor: Jose Alfonso Artero Guerrero

September 26, 2017

Numerical Study of a One Stage Gas Gun

Final thesis for the degree **Bachelor in Aerospace Engineering**
Tutors:

- Jose Alfonso Artero Guerrero
- Jesús Pernas Sánchez

Abstract

Gas guns of either one or two stages are very useful and common tools during the testing of aircrafts and spacecrafts, in such a way that they must be able of reproducing many different impact situations, from a bird impact on a civil aircraft to a meteorite hit on a satellite.

In order to adequately reproduce each situation during and impact test, the most important parameters to be controlled are muzzle speed and projectile mass and dimensions. Because of this, the appropriate gun should be used when running and impact test according to its design features.

In this paper, the different issues of a Single stage gas gun are to be discussed and analyzed. The different parts of the gun are to be studied with the objective of optimizing the design and understanding its performance. To do so, mainly numerical calculations will be performed by means of software LS-Dyna, specifically the new compressible solver tool. Aditionally, an experimental prototype devoted to support the calculations will be designed and built.

Contents

List of Figures

1 Introduction

One of the most important tendencies nowadays in aerospace industry is to reduce the emissions of the aircraft to the environment, for example, SESAR (Single European Sky ATM Research) objective is to modernize the ATM network to reduce the environmental impact by a 10% per flight [1], Aircraft manufacturer companies as Airbus are implementing new aircraft models as the A320NEO family, which reduces up to a 50% the emissions of NOx by means of more efficient engines [2], other possibility is to reduce the energy required to propel the aircraft, which in fact can be achieved by reducing the weight of the plane.

The weight reduction of the aircraft obviously has a direct impact on the way its structure is designed, this is of special interest for the scope of civil aviation, where the cost of fuel is one of the main expenses incurred by customers when buying a ticket. Considering that as an average, the 40% of the actual weight of the aircraft is represented by the fuel, an important reduction in the structural weight would lead to the reduction of the fuel required and to less emissions.

In the design phase of the aircraft, the different loads that the structure will experiment during operation must be considered so the structural integrity can be assured with the minimum weight possible. In the last years, the tendency is to increase the Carbon Fiber composites and Glass Fiber composites for the structure and other components of the aircraft due to their mechanical properties and good performance. Although the advantageous performance of composite materials supporting loads in the same directions as the fibers, one of the most critical aspects to be taken into account is their vulnerability to out-of-plane impulsive loading as a result of the reduced thickness of the laminate configurations and the brittle behavior of the fibers. If impulsive loading is produced by high-speed impacts, the study of this problem takes on importance in the aeronautical field. During take-off and landing, it is not uncommon that the aircraft is hit by stones, tire fragments, etc. Similarly, during flight, the aircraft can be hit by birds, hail, ice, or sheds from the turbine blades. [3]

Therefore, impact analysis has become a relevant topic not only for the regulatory point of view but also for researching about aeronautical safety. The regulatory certification requirements for European Aircraft (Joint Aviation Requirements, JAR) and for the American Federal Aviation Regulations (FAR) account for specific requirements so failures caused by impact can be prevented and for guaranteeing a certain level of functioning in the event of an incident, so that aircraft can continue to fly until landing safely [4]. Similarly, from the current EU Framework Programme for Research (FP7), as well as the European funding framework for scientific projects, Horizon-2020, for which one of the main priorities is to promote the research on aeronautical safety. [5]

Aviation authorities demand that every component of the aircraft facing the direction of flight (wing leading edges, fuselage, tail wing, engines and window frames) have a certain resistance to bird impact which can be demonstrated through certification, which is explained from the fact that bird strike accounts for around 90% of all incidents related to structural damage due to impact on aircraft. [6]

Certification testing, carried out with real birds in flight conditions, is not only very hard to recreate but also very costly. In order to certificate the aircraft, many aeronautic companies use artificial birds or substitute material in pre-certification experimental tests. [7]

Similarly to bird strikes, ice impact has become a subject of regulation for the aeronautical authorities (JAR-E 970), especially in aircraft with open-rotor engines belonging to the new generation of aircraft used for medium-range routes. [8] Impacts of tire fragments, which normally occur at speeds rounding the 100m/s during take-off or landing phases, and their influence on the design of aeronautic structures took on particular importance after the repercussions of the accident involving the supersonic Concorde plane in Paris in the year 2000, which was caused by a tire fragment impact on one of the fuel tanks. [9]

Not only the impact testing is important for aviation, at the NASA's Remote Hypervelocity test laboratory at White Sands, New Mexico, micrometeoroids and orbital debris impacts on spacecraft shielding, components, and materials in various test configurations are simulated, completing over 600 shots per year with low costs. [10] This gives an overview of the importance of the development of impact testing to improve safety not only on civil aviation but in many other fields as spacecrafts or high velocity rail vehicles.

1.1 Objectives

The scope of this paper is to study the performance of one stage gas guns of different characteristics, so the effect of modifying some of the parameters involved in the actioning of the gun, as reservoir pressure, projectile dimensions, shape, mass, proppellant gas and finally, the implementation of a convergent-divergent nozzle, can at least be qualitatively determined and understood.

To do so, numerical models are to be prepared with a new compressible solver which allows the accurate study of high speed flows as the ones characterizing the air gun located at UC3M facilities and the ping pong gun which is to be designed and built, so real results obtained with them can be compared with the numerical models, allowing to understand the final performance from the evolution of the flow inside the gun.

After some theoretical background, the methodology and the results obtained, first with the UC3M air gun and then with the ping pong gun are explained in detailed along next sections.

1.2 Gas Guns

Gas guns have been used for impact testing for quite a long time, indeed, the first two-stage guns appeared right after the end of Second World War [11] and together with Single stage guns, they have become one of the most used laboratory equipment for launching projectiles of a wide range of shapes, dimensions and masses at speeds which can go from just a few meters per second to more than 7500 meters per second, twenty-two times the speed of sound at sea level.

Notice that these speeds refer to muzzle speeds, which means, the speed that the projectile being launched has when, after going through the barrel, passes through the mouth of the gun. As shown later in this paper, this fact is very important as many of the actual light gas guns make use of having vacuum inside the barrel, so the projectile can be accelerated without aerodynamic drag, nevertheless, when the projectile gets out of the barrel and performs a free-flight, it is rapidly decelerated due to air friction. Considering that, at least the test section of some light gas guns (the very expensive ones) is placed within a vacuum chamber so the projectile is not affected at any time by aerodynamic drag.

During this paper, the different discussions will focus only on Single stage gas guns, so the main differences between One and Two stages guns may be clarified. Both work by means of a gas, which can be air, helium, hydrogen, nitrogen, etc., that is compressed within an insulated tank to several times the atmospheric pressure and then, this gas is released so it pushes the projectile accelerating it

through the barrel.

The main difference lies in the way the propellant gas is compressed for each one. For the Two-stage gun, a detonation is produced with a small amount of gunpowder (similar to a gunshot) at the first stage, so the energy produced is devoted to compress some light gas as hydrogen or helium, so when this gas reaches an specific pressure, it breaks a seal and the gas is released to propel the projectile. On the other hand, single stage gas guns just compress the propellant gas by means of a compressor, so the speeds which can be reached are much smaller for this type of guns.

Regarding the gases which are used to propel the projectile, they are typically light gases for two main reasons. The first one is that light gases have very low molecular weights, so they can be easily compressed to the high pressures which are required to launch projectiles at high velocities in an efficient way. The other reason is that the speed of sound is higher in these gases than it is in air, which is a limiting parameter for gas guns as it will be demonstrated in the following subsection. Nevertheless, air guns are still widely used within the scope of impact tests.

Finally, it has to be mentioned that for the Two-stage gas guns, the light gas which is to be compressed has not only its pressure increased, but also its temperature. This is due to the high amount of energy released by the gunpowder detonation, which can be considered to isentropically compress the light gas increasing consequently its temperature. This is a very important issue, as the temperature increment has a direct impact on the speed of sound in the medium as deduced from next equation, where γ is the heat capacities ratio of the gas, R the gas constant and T, p and ρ the temperature, pressure and density respectively.

$$a = \sqrt{\gamma RT} = \sqrt{\gamma \frac{p}{\rho}} \tag{1}$$

From the previous equation it can be seen what Two-stage light gas guns do to reach projectile supersonic speeds, as when increasing not only the gas constant but also the temperature, the speed of sound is notably increased.

For the case of single stage gas guns, there is typically no increment in the temperature of the propellant gas, as the process of compressing the gas is much slower so it can not be considered an adiabatic process, in fact it is an isothermal process, which implies that although the pressure is increased in the reservoir, the temperature is kept almost constant, as it does the speed of sound. So the most common way of obtaining higher speeds in single stage gas guns is by modifying the gas properties in equation 1, which implies using gases as helium or hydrogen which even though they have similar specific heat ratios, their density ρ is about

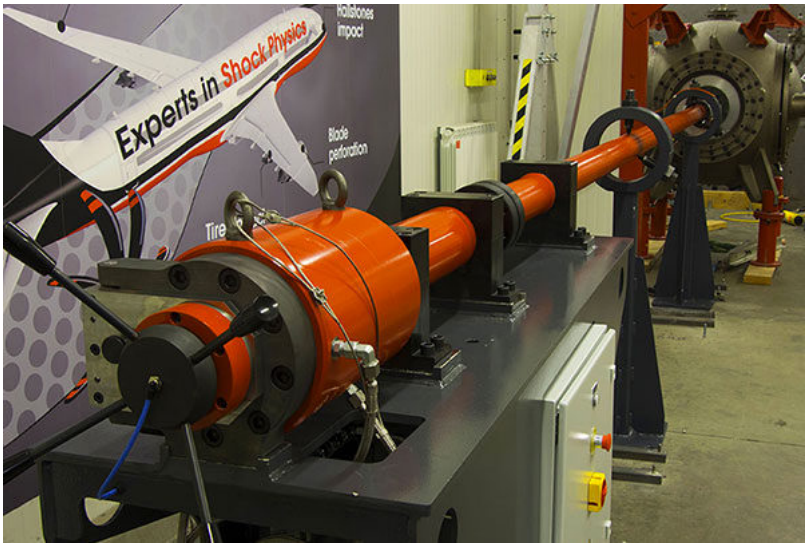

Figure 1: Thiot Ingenierie TITAN single stage gas gun. [12]

one order of magnitude smaller than that of air.

Notice that, although if helium is being used as a propellant gas for a single stage light gas gun and projectile speeds around 1000m/s are obtained, this does not actually mean that the velocity is supersonic, in fact, the flow speed within the barrel is also limited by the speed of sound wave propagation within helium. In order to really reach supersonic speeds, a gas gun counting with a convergent-divergent nozzle is proposed, similar to a rocket nozzle or a supersonic wind tunnel. In the later, several different issues are to be discussed about design considerations and the feasibility of the system.

1.3 Theoretical background

1.3.1 Nozzle design

To understand the limitation of the speed of sound, let's first consider a reservoir discharging a compressed gas through a convergent nozzle. It can be assumed that the mass flow rate $\dot{m}$ is constant along the symmetry axis of the nozzle and that the velocity is parallel to this axis, so the variables characterizing the mass flow will be function only of the coordinate along the axis of the nozzle.

$$\dot{m} = \rho u A \tag{2}$$

So if the mass flow rate must be kept constant along the nozzle, as the cross sectional area A is reduced, the flux density j (equal to the density times the velocity) must increase. It can also be easily deduced that the maximum flux density is obtained at the narrowest part of the nozzle, because if this was not the case, it would mean that there exists a point where $A > A_t$ with a flux density higher than that at the minimum cross section, which is impossible, as the mass flow conservation would not be fulfilled.

The relation between flow velocity and cross sectional area (and also Mach number) can be easily obtained by means of mass conservation, momentum conservation and isentropic flow relation:

$$\textbf{Mass conservation:} \quad \dot{m} = \rho u A \quad \Rightarrow \quad \frac{d\rho}{\rho} + \frac{du}{u} + \frac{dA}{A} = 0 \tag{3}$$

$$\textbf{Momentum conservation:} \quad \rho u du = -dp \tag{4}$$

$$\textbf{Isentropic flow:} \quad \frac{dp}{p} = \gamma \frac{d\rho}{\rho} \quad \Rightarrow \quad dp = a^2 d\rho \tag{5}$$

Combining 4 and 5 it yields:

$$-M^2 \frac{du}{u} = \frac{d\rho}{\rho} \tag{6}$$

Which can be expressed as:

$$\frac{d\rho}{du} = -\rho \frac{u}{a^2} \tag{7}$$

and substituting $d\rho/du$ into $d(\rho u) = \rho du + u d\rho$, it yields:

$$\frac{d(\rho u)}{du} = \rho(1 - \frac{u^2}{a^2}) \tag{8}$$

This implies that, as the velocity increases along a streamline, the mass flux density increases in a subsonic regime, whilst if the Mach number is greater than one, the flux density behaves the opposite way.

Now when introducing equation 6 in the mass conservation equation it finally leads to the well known:

$$(1 - M^2)\frac{du}{u} = -\frac{dA}{A} \tag{9}$$

From these results, it can be concluded that in the narrowest part of the nozzle the flux density is maximum and that at that point the velocity is equal to the local speed of sound. Therefore, from previous equation it can be deduced that for a Mach number equal to 1, the only way to keep increasing the speed is by changing the sign of the right hand side of the equation, which means that the cross sectional area must increase to reach supersonic velocities.

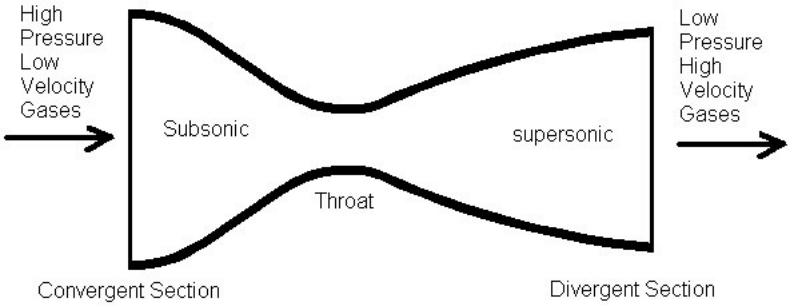

Figure 2: Convergent-Divergent nozzle scheme. [13]

Keep in mind that for the convergent-divergent nozzle, the flow is subsonic ($M < 1$) before the throat and keeps accelerating until it reaches $Mach = 1$ at the narrowest cross section, then, for the Mach number to be greater than 1, the left hand side in equation 9 must change its sign, so the derivative of the cross sectional area must do the same so that the flow keeps accelerating during the supersonic expansion.

1.3.2 Nozzle Flows

Within this section, the different flows and phenomena appearing in convergent-divergent nozzles for different conditions are to be studied. The following demon-

stration will show the effect of the geometry of the nozzle, specifically the ratio of throat and exit areas in the flow. Keep in mind that at the throat of the duct, the Mach number is equal to 1, so the subindex t in this case also implies sonic conditions.

$$\rho_t u_t A_t = \rho u A = constant \tag{10}$$

Considering that at the throat $u_t = a_t$:

$$\frac{A}{A_t} = \frac{\rho_t}{\rho}\frac{a_t}{u} = \frac{\rho_t}{\rho_0}\frac{\rho_0}{\rho}\frac{a_t}{u} \tag{11}$$

Where the subindex 0 refers to the stagnation quantities, which are constant throughout an isentropic flow as it is the case. The isentropic relations are:

$$1 + \frac{\gamma - 1}{2}M^2 = \left(\frac{\rho_0}{\rho}\right)^{\gamma-1} = \left(\frac{p_0}{p}\right)^{\frac{\gamma-1}{\gamma}} = \frac{T_0}{T} = \left(\frac{a_0}{a}\right)^2 \tag{12}$$

So squaring equation 10, substituting ratios from previous equations and operating algebraically to simplify, it yields the expression which relates the local Mach number at any point of the duct with the area ratio at that cross section. [14]

$$\left(\frac{A}{A_t}\right)^2 = \frac{1}{M^2}\left[\frac{2}{\gamma+1}\left(1 + \frac{\gamma-1}{2}M^2\right)\right]^{(\gamma+1)/(\gamma-1)} \tag{13}$$

Recall that for an isentropic flow, is not possible to have $A < A_t$ as the Mach number in the throat is equal to one and the flux density is maximum in that point, so the area ratio of the left hand side is greater than one. One important result from this formula is that for any area ratio, there exists two different Mach numbers which fulfill the equation, one subsonic and other supersonic. It can be deduced that the Mach number of the two possible ones that hold depends on the pressure ratio of the duct. Both possibilities are shortly studied here but obviously, the supersonic is the one which will be implemented for the gas gun.

Assuming that the geometry of a convergent-divergent nozzle is known, so the area ratio A/A^* is also known (where the star means sonic conditions), two Mach numbers and its corresponding pressure ratios can be computed by solving equation 13. Depending on the pressure difference existing across the duct, different flows can be described.

If the pressure ratio p_e/p_0 is close to 1, meaning very small pressure difference, a low speed flow would be produced across the duct, accelerating in the convergent

part of the nozzle up to the throat where the flow density would be maximum as well as the Mach number. Nevertheless, it would be smaller than one, so in the divergent part, the flow will expand and decelerate. Obviously, the pressure would decrease in the convergent part and increase in the divergent.

Suppose now that the pressure difference is increased in such a way, that at the throat, sonic conditions are reached, so the flow is supersonically accelerated in the divergent part. Keep in mind that there exist just one pressure ratio which leads to supersonic isentropic flow in the nozzle (for the subsonic case there exist infinite isentropic solutions). Assuming supersonic flow in the divergent part, if the pressure ratio across the duct for a given fixed shape of the nozzle is different from the one obtained with equation 13 and the isentropic relation

$$1 + \frac{\gamma - 1}{2} M^2 = \left(\frac{p_0}{p} \right)^{\frac{\gamma - 1}{\gamma}} \tag{14}$$

the flow would not be isentropic anymore and either shock waves or Prandtl-Meyer expansion waves appear depending on the actual pressure ratio.

Lets assume that at a first instance, the pressure ratio across the nozzle leads to isentropic subsonic flow in the whole duct, but now, the pressure ratio is decreased so sonic conditions are reached at the throat, such that $\dot{m} = \rho^* u^* A^* = \rho^* u^* A_t$. Therefore, if the pressure at the exit is further decreased, the Mach number would still be equal to 1 at the throat and the mass flow rate would remain constant, in that situation the flow is said to be choked.

Although the flow would not change before the throat when the nozzle is choked, as mentioned before, different things can happen in the divergent part depending on the exit pressure. For the case where the pressure ratio is smaller than the one of isentropic supersonic solution, the pressure difference in the divergent part would not allow the flow to be isentropic all the way, so a normal shock wave appears to increase the pressure and adapt it to the exit pressure. Notice that although the flow is isentropic before and after the shock wave, the entropy increases across the discontinuity. If the pressure gradient is further reduced, the normal shock wave moves to the exit section of the nozzle.

Finally, if the back pressure ratio (pressure of the surroundings where the nozzle discharges) is equal to the ratio of the supersonic isentropic solution, the flow at the exit is said to be matched, so the nozzle discharges smoothly without any discontinuity. If the back pressure is slightly increased from last case (but still smaller than the case with the shock wave at the exit), a set of oblique shock waves appear at the nozzle exit, whereas if the back pressure is further reduced, the flow at the nozzle exit suffers expansions so the pressure reduces up to the

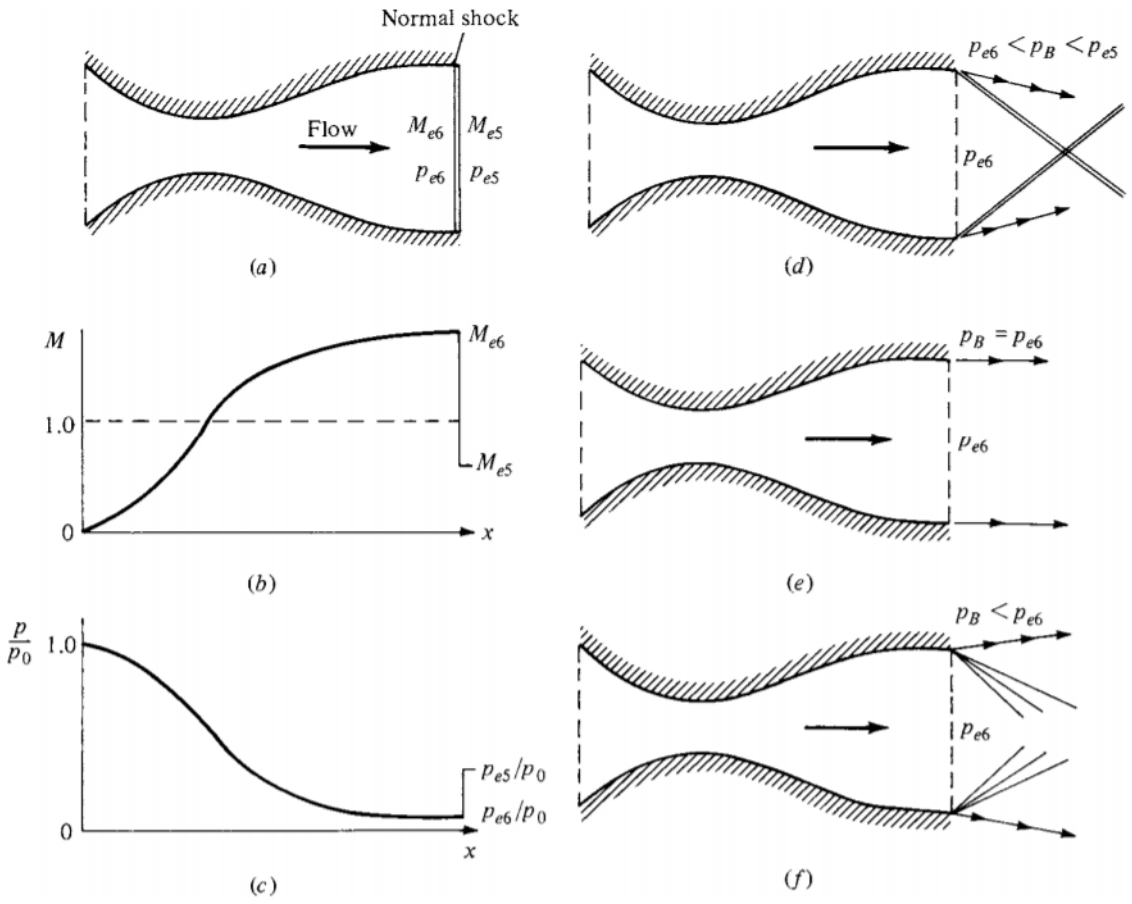

Figure 3: Supersonic nozzle flows with waves at the nozzle exit: (a), (b), and (c) pertain to a normal shock at the exit, (d) overexpanded nozzle, (e) isentropic expansion to the back pressure equal to the exit pressure, (f) underexpanded nozzle.[14]

surroundings one. Obviously, for the implementation of the convergent-divergent nozzle in the gas gun, the most desirable situation of all of the above is the one where the flow is supersonic and perfectly matched at the exit of the nozzle without any discontinuity (entropy keeps constant), represented in figure 3 (e) and in figure 5, which also shows the Mach number and pressure variations across the nozzle.

1.3.3 Nozzle exhausts into constant-area duct

The model of the gas gun that this paper is studying, counts with a high pressure gas reservoir which discharges supersonically through a convergent-divergent nozzle into a long tube of constant area that is the barrel of the gun, where the

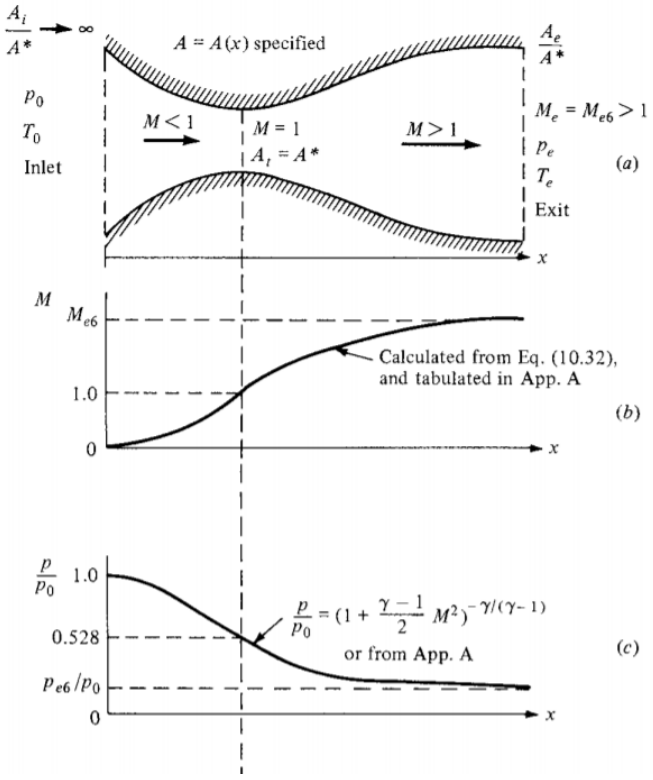

Figure 4: Isentropic supersonic nozzle flow. [14]

projectile is accelerated. It was previously studied that the most desirable flow in the duct would be the supersonic isentropic solution, nevertheless it may be difficult to achieve that matched flow. This is the same problem that supersonic wind tunnels encounter.

The objective of supersonic wind tunnels is to achieve a supersonic flow ($M > 1$) within a test section where the model to be studied is located. Supposing the test model is located inside a room with ambient pressure and the nozzle is expected to exhaust a matched supersonic flow at $M = 3$ so the model can be tested without having any shock wave, the required pressure ratio would be equal to 36.73, which implies that the pressure at the reservoir must be 36.73 atm. This pressure, which in fact is difficult to obtain by means of a compressor, is very expensive to be achieved.

The solution comes from the development of different flows of the previous section. Consider now that at the exit of the nozzle, a constant area duct is placed, then the pressure gradient can be configured in such a way that a normal shock wave appears at the end of the duct, but all the way upstream the flow is isentropic without any discontinuity. In this case, the pressure before the shock wave

can be obtained from normal shock relations, [14] that for a Mach number equal to 3 in the constant area duct, means a pressure jump of $p_1/p_2 = 0.097$ across the shock, this implies a pressure at the nozzle exit of just 0.097 atm, so now the reservoir pressure to achieve Mach 3 is just of 3.55 atm, much smaller and feasible than the 36 atmospheres for the matched discharge.

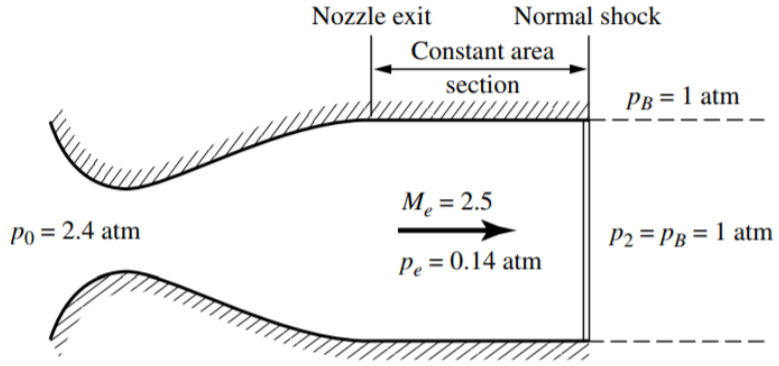

Figure 5: Nozzle exhausting into a constant-area duct with a normal shock-wave at the exit for Mach number equal to 2.5 in the constant area section. [14]

This result can be implemented in the gas gun if the barrel is taken as the test section of the wind tunnel. The compressed gas will accelerate supersonically at the nozzle and then it will propel the projectile through the barrel without any discontinuity in the flow up to the muzzle, where the projectile leaves the barrel at supersonic speed. Nevertheless, in order for this to always hold, several assumptions have been made, these are frictionless flow through the duct and no heat transfer. Although heat transfer is typically avoided with insulated guns, the effect of friction has to be taken into account.

Fanno flows describe adiabatic flows through constant area tubes where friction is considered [15]. The most important effect of friction in the flow is that, as it increases the entropy, if the flow is supersonic, it is decelerated to Mach equal to 1, which is the condition of maximum entropy (for subsonic regime the flow does the opposite and accelerates, so it can get choked for long enough pipes). Decelerating the flow implies that the shock wave that was expected to be located at the exit of the constant area duct, now is displaced at some distance L^* from the nozzle exit, such that if the distance $L^* = L$ (being L the length of the tube) the normal shock wave will appear at the exit of the tube, which was the most desirable case for the gas gun design.

Notice that these conclusions are deduced for steady flows, which in principle, it is not the case of the gas gun. In practice, the projectile travels the barrel before the

propellant gas, and if it goes supersonic, when the flow gets choked due to friction (if it does) it would not see any perturbation of the flow upstream. Nevertheless, in the numerical models, some of these phenomena are intended to be observed, so the capabilities of the software used can be identified and discussed.

1.3.4 Flow around the propelled projectile

The flow inside the gun may be divided in different parts which are, the convergent-divergent nozzle, the flow in the duct before reaching the projectile and the flow around the projectile. The first two have been previously considered, so in this section, the flow around the projectile is to be commented.

Later on, two main projectile shapes are to be implemented in the models, for the 18m long gun, there is no bore distance (space between the projectile and the inner wall of the barrel) so there is nothing to say, nevertheless, for the spherical projectile, it has been modeled in such a way that there exists a small difference between ball diameter and caliber of the gas gun.

Lets consider the ping pong gun case. Along the barrel the flow has a velocity of the order of $100m/s$ to $400m/s$, the density is around $1kg/m^3$ to $2kg/m^3$, so for a diameter of 3.6cm, the Reynolds number is of the order of 2000000. This means that in the Navier-Stokes equations, the convective terms are big compared to diffusive terms (mainly viscosity), so the flow is said to be turbulent (recall that for $Re > 4000$ the flow is considered turbulent, whilst for $Re < 2500$ is said to be laminar).

$$Re = \frac{\rho U D}{\mu} \tag{15}$$

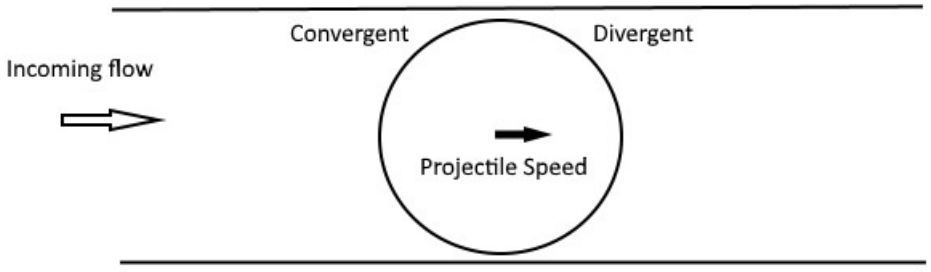

Figure 6: Ball acting as a convergent-divergent section

It has to be considered that some gas flows between the ping pong ball and the inner wall of the barrel, so when computing there the Reynolds number, now the diameter is much smaller, of the order of 0.5mm, and the velocity is now slightly higher as the flow is accelerated when passing through the bore. These yield a Reynolds number around 30000, that is much smaller but still shows the turbulent character of the flow. The thickness of the boundary layer is of the order of the radius of the ball over the square root of the Reynolds number, so it would mean a boundary layer thickness 1/173 the radius of the ball. Considering the last, the flow around the ball during the shot can be considered as a turbulent flow through a convergent-divergent section where one of the walls is moving. Indeed, it is quite complex to approach this problem analytically, that is why numerical models are used to explain the behavior of the flow passing around the ball.

2 Equipment and Method

2.1 LS-Dyna

LS-DYNA is a general-purpose finite element program widely used for complex problems of different industries as aerospace, bioengineering, military, manufacturing and others. More specifically, the solver which is going to be used for the numerical models is the Compressible Fluid solver, capable of solving high speed flows with presence of shock waves or other non-isentropic solutions.

This compressible solver is based on the space-time conservation element and solution element or CE/SE method, which was originally proposed and developed in NASA Glenn Research Center. This method has been built from fundamentals, and not as a modification of any previously existing method, so it notably differs from any other well-established solvers. The CE/SE method is a second order explicit scheme and implements several innovative features as flux conservation in space and time (locally and globally) allowing physical reality scenario to be retained in regions of discontinuities. [16]

Just to mention that, although LS-Dyna is widely used nowadays for many physical problems, the CE/SE solver seemed to be in continuous development up to date, for instance, during the implementation of the numerical models of the gas gun described later on this paper, several bugs where found in the preprocessor used to design the model, so they were fixed by developers after this project. In order to ensure the correct performance of the software, several simulations of each design were run to double check the results. In addition, these numerical results were contrasted with data retrieved from tests at UC3M facilities with air gun. The LS-Dyna model was designed with the same characteristics as this gun for an accurate comparison.

LS-Dyna works with a keyword (.k file) containing all the information about the model which is read at the beginning of the simulation, this keyword is composed by "cards", each of them regarding to some specific aspect of the model, from the "Node card" containing the coordinates of every node of the grid, to the "Mat card" about the mechanical and physical properties of the projectile material. This .k file can be easily edited with a text editor so any characteristics as shell or solid elements or any quantity as density, initial pressure, etc, can be easily identified and modified. One example of the reduced input for the ping pong gun LS-Dyna model is shown in appendix B.

2.2 Numerical models

Before detailing each specific model which have been design with LS-Dyna during this project, the general issues of the models are to be defined now.

As all of the models are gas guns, several aspects are present on every model, which are the reservoir, the barrel and the projectile. It was decided to model them taking advantage of the axis-symmetry of the problem, so they are designed as in the picture below.

Figure 7: Basic gun design

Once the 2D surface has been defined, the mesh of the model is to be constructed. Notice that the size of the shell elements has been selected taking into account both computational times and convergence of the results after some simulations (this will be discussed later on this paper). LS-Dyna automatically builds an unstructured grid with both triangle and quadrilateral elements to adapt the mesh to the irregularities of the 2D surface, nevertheless, at this step the elements must be divided into smaller ones (figure 8) so every one of them is a quadrilateral element (CE/SE can only deal with quadrilateral elements in 2D), if not, the solver will not be able to carry out the simulation and it will lead to an error.

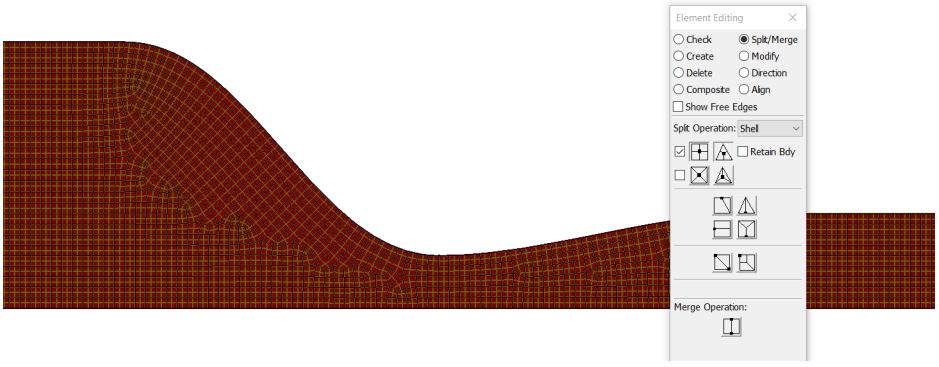

Figure 8: Mesh element generation for the nozzle shape

With the grid properly defined, the boundary conditions have to be settled. The set of segments of the long edge at the bottom of figure 7 are declared as the axisymmetric set (represents the edge of axial symmetry). The small vertical edge at the right of the figure, which represents the muzzle of the barrel, is declared

as the non-reflective set, this boundary condition (NBC) provides an artificial computational boundary for an open boundary that is passive. Finally, the rest of the edges are declared as Solid Wall boundary condition.

Once the gun has been modeled, it is time for the gas properties. Gases in LS-Dyna are defined by means of an equation of state of ideal gases card containing the constant pressure and constant volume heat capacities of the gas. Also, the initial variables of the gas have to be defined by means of initial pressure and temperature. It is also possible to add a "Mat gas card", where Sutherland's coefficients of the formula for viscosity can be determined.

At the moment of defining the projectile, it has to be consider that the main objective of the project is to analyze the gun performance, regardless of what happens to the projectile, so it is defined as a Rigid not deformable material, for which only the density has to be determined.

Finally, some controls cards are declared regarding, initial timestep and CFL (Courant Friedrichs Lewy condition), inviscid or viscous flow, 2D axisymmetric, immersed boundary for the FSI (fluid structure interaction) or stability parameters.

The models explained in next sections are basically small variations of the general model. The most important modifications are the change of dimensions between different guns, the implementation of an opening valve and overall, the implementation of the convergent-divergent nozzle.

3 Air gas gun 18m barrel

The first idea at the beginning of this project was to carry out a numerical study of one of the light gas guns located at UC3M facilities. By the moment this project was started, ballistic tests with the air gun were taking place, so it was decided to build a numerical model to study the gun. These are the specifications of the system:

- Propellant gas: Air
- Barrel length: 18m
- Caliber: 60mm
- Reservoir: 1.5 m^3 at 6 bar

With those specifications, the model was implemented into LS-Dyna following the process mentioned in previous section. To start, the simplest model was designed, just a cylindrical reservoir connected to a barrel with a cylindrical projectile located at the entry of the barrel. Several simplifications apply to this model, the gun is assumed to be insulated, there is no valve between the reservoir and the barrel and there is no friction between the sabot and the wall, the bore distance (difference between the sabot diameter and caliber of the barrel) is also zero, whilst in reality always exist some tolerance between projectile and barrel. Also mention that for this first example the flow is treated as Inviscid.

Figure 9: Air gas gun axis-symmetric model

For this first case, the projectile weights 33 grams, so after setting the density of the material and the initial pressure and temperature of the reservoir, the program begins the simulation. Notice that the initial temperature of the reservoir is set to 263 K, this is because the pressurized air is not obtain with a compressor but it comes from a bigger tank of $3m^3$ and 10 bar, so as a first approach, considering an ideal gas expansion and doing some calculations, the resulting temperature is about $-10°C$, which makes sense given that some frost appear on the tanks and tubes when filling the reservoir.

In the figure below they are shown some results concerning pressure and temperature right after the valve is opened (keep in mind that this model has no valve implemented, so it is assumed that the valve is instantaneously erased). Notice that the pressure is expressed in $g/(\mu s^2 cm)$ and temperature in kelvin. The units

have been selected like this on the advise of LS-Dyna developer to adjust the units for the scale of the case of study. From now on, this units for distance (cm), time (μs) and mass (g) will be kept for the rest of the paper unless specified in a different way.

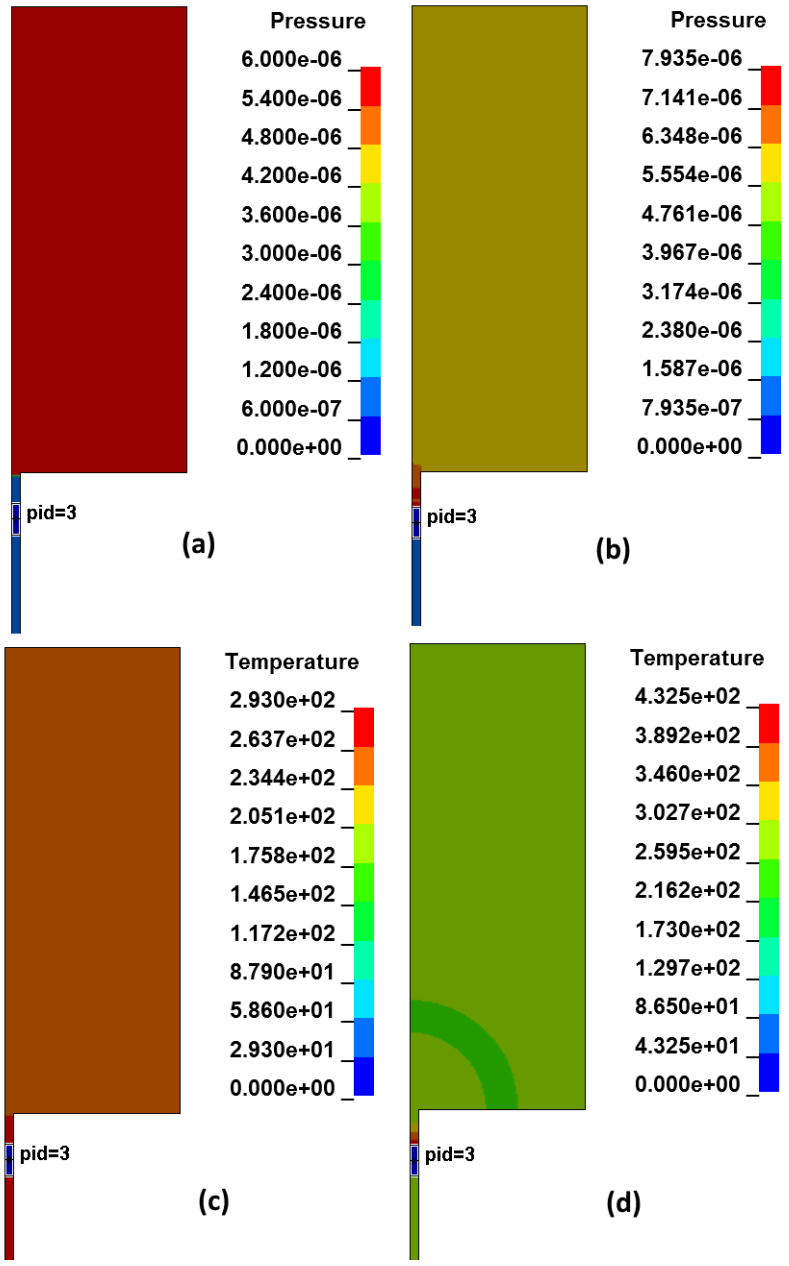

Figure 10: Pressure contour at $t = 0ms$ and $t = 1ms$ (a) and (b). Temperature contour at $t = 0ms$ and $t = 1ms$ (c) and (d).

Figure 10 shows that as there is no bore distance between projectile and barrel, when the high-pressure air tries to get out of the reservoir, it is blocked by the

sabot so it starts pushing. Here, it can be seen how right after the gas is released, as the projectile is in rest, the pressure and temperature at its back are notably increased, in reality this does not happen, as the bore distance is fixed in such a way that some gas surpasses the sabot so this increase in pressure and temperature is not as sharp as here.

Figure 11 shows the vorticity which appears at the barrel entry and around the moving projectile. The vorticity of the reservoir exit extends to the whole cross sectional area of the throat, this obviously contributes to kind of obstruct the outgoing mass flow through the reservoir exit. This effect is commonly avoided by rounding the corner of the entry, it will be seen on later cases how it is almost completely suppressed by connecting the tank and the barrel by means of a nozzle with entry section equal to the tank cross section, so there is no corner for vorticity to be formed.

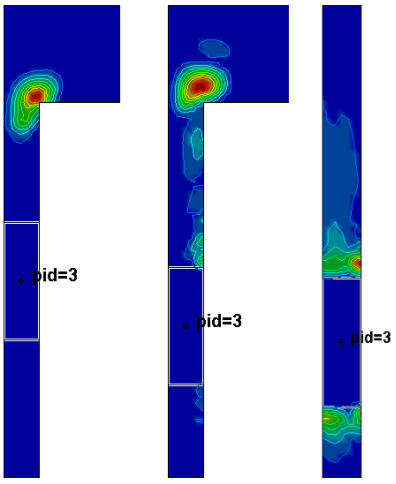

Figure 11: Vorticity at the barrel entry and around sabot at different time-steps.

Next figure shows the speed that the projectile has at every position along the barrel of the gun. It can be seen how as the gas is released from the reservoir, the projectile suffers a high acceleration reaching the 260m/s in just 5 meters, on the other hand, the speed slightly changes in the rest of the barrel. This graph is very useful as it can be used to optimize the length of the barrel, notice that a gun of 5 meters against one of 18 meters makes a big difference both in cost and space to operate the gun.

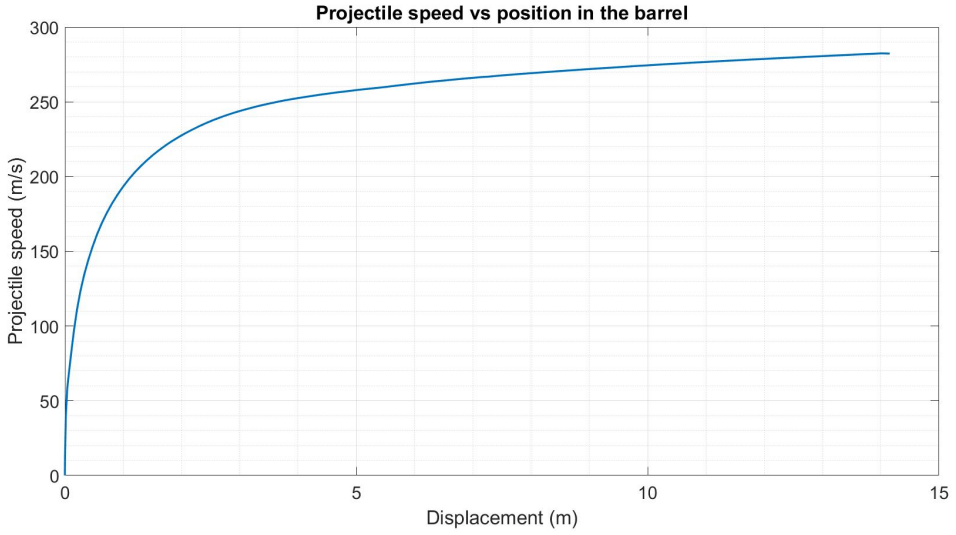

Figure 12: Speed of the projectile along the gun barrel

3.0.1 Air gas gun with valve 18m barrel

Now, an axial valve has been introduced in the model, so the effect of gradually opening the valve can be implemented. Notice that the time that the projectile requires for traveling the whole barrel is very small, of the order of 0.012 seconds, so even if the valve is released very fast, the opening time has an impact on the performance.

To simulate the valve, two rigid bodies have been introduced in the model so the valve acts like a piston. The yellow body in figure 13 is fixed in space and the brown one is the piston which is being retracted with a prescribed motion previously settled. In the initialization of the model, the piston is said to be retracted 9 cm in 0.02 s, meaning an opening speed of 4.5 meters per second. Notice that as no data was available from gas gun manufacturer, this opening time is arbitrary and it has been implemented just to compare the effect with respect to the no valve case.

3.0.2 Air gas gun with valve 18m barrel and vacuum

With the valve implemented, the model is very similar to the actual one, nevertheless, it was decided to study the effect of making vacuum inside the barrel so this feature may be introduced in the real gun. In that way, a vacuum of 99% was defined in the whole barrel, so when the projectile is being propelled by the high pressure gas, it does not seen any aerodynamic drag. Apart from this, the same simulation was run but instead of determining the flow as inviscid, it was

Figure 13: Gun model with valve

set as viscous, so the effect of viscosity can be analyzed.

The way LS-Dyna models viscosity is by means of the coefficients of Sutherland formula, where C_1 equals to $1.458e^{-6}\ kg/msK^{1/2}$ and C_2 equals to $110.4K$ for air at moderate temperatures. [17]

$$\mu = \frac{C_1 T^{3/2}}{T + C_2} \tag{16}$$

Next three figures show the performance of the gun in terms of speed of the projectile along the barrel, the flow properties evolution at the barrel entry and also the Mach number at that position. In the projectile speed curve it is shown that as expected, the inviscid model with vacuum in the barrel has a muzzle speed around 500m/s, a 25% higher than the standard model, but on the other hand, when considering the effect of viscosity, the muzzle speed is reduced a 20% with respect to the previous case.

Figure 15 shows the variation of velocity, density and temperature with time at a node located at the barrel entry and the axisymmetric axis for the case with vacuum and viscous flow. The red dashed line at the beginning of the graphs represents the variation of the properties when the valve is still located over the node where these quantities were measured, that is why they show unrealistic results for that period of time. Once the valve is completely opened, the evolution of the three quantities shows a sharp increase before stabilizing. Notice that the flow temperature starts being so small because at the beginning of the simulation, the node where temperature is being measured is in vacuum, nevertheless, when the compressed gas is released the temperature reaches a maximum and then decreases due to the expansion of the gas. Notice that the flow speed is stabilized at just 180m/s by the moment the projectile leaves the barrel with a muzzle speed of 400m/s as shown in previous figure, this means that the flow is still being accelerated within the barrel as it follows the projectile (as there is

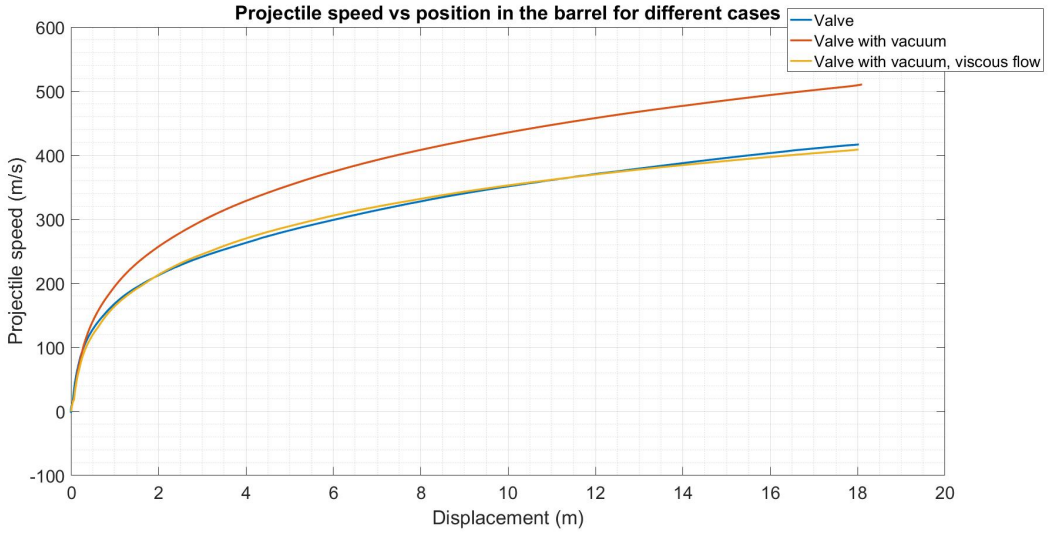

Figure 14: Comparison of speed evolution of the projectile along the gun barrel for different cases

no bore, the fluid right before the sabot must be at the same speed as it is. In figure 16, the Mach number evolution at the same node shows that the flow does not reach sonic conditions at the barrel entry, which is consistent with the fact that the fluid is being accelerated in the barrel, as explained in section 1.3.3, for viscous subsonic flow in constant area ducts, the flow accelerates until reaching Mach 1, so it can get choked at some point of the duct if it is long enough.

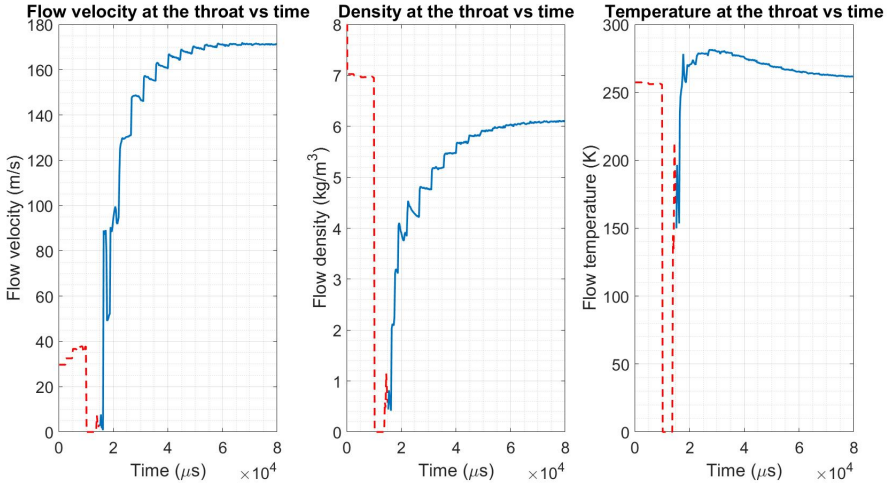

Figure 15: Velocity, density and temperature at node located at the symmetry axis at the barrel entry

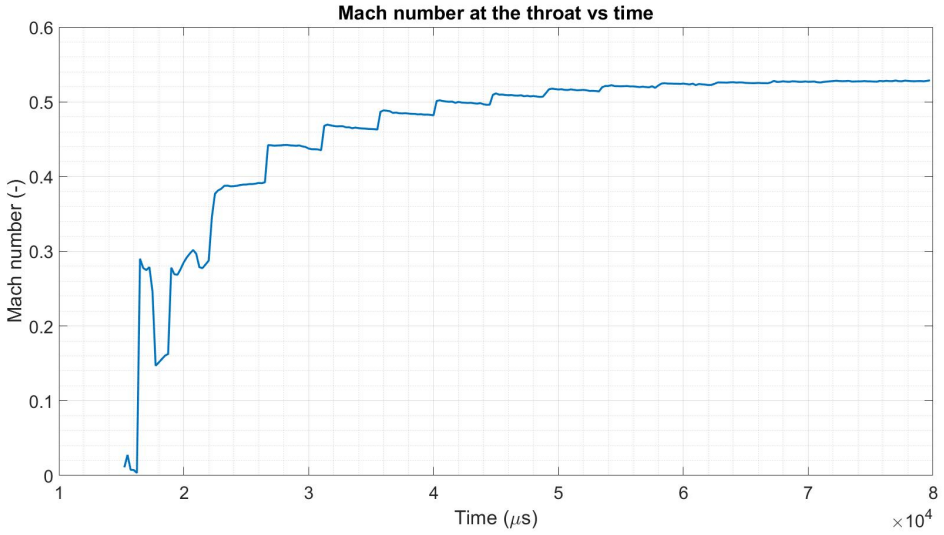

Figure 16: Mach number at node located at the symmetry axis at the barrel entry

3.1 Air gas gun with valve 18m barrel with 140g projectile

In this section, the exact shooting conditions of the air gun at UC3M facilities have been reproduced so the pressure-velocity curve can be compared for the experimental and numerical cases. The same model has been solved for both inviscid and viscous flow and for several reservoir pressures. Notice that the Reynolds number is of the order of 1 million, so the flow is obviously turbulent, so the viscous effect which would have an impact on the result should be only the viscosity inherent to the turbulence.

In figure 17 it is shown that whilst for the viscous model the speed of the projectile seems to nearly stabilize at the last meters of the barrel, the inviscid case apparently keeps on increasing almost linearly at the last meters. Now when comparing results for different reservoir pressures for the viscous case shown in figure 18, it is clearly seen that the smaller is the pressure, the sooner the projectile speed stabilizes, so for low shooting pressures, the optimal length of the gun is smaller. These two figures depict the behavior of the projectile inside the gun so it allows to optimize the length of the barrel, nevertheless, figure 19 shows a more important result: the actual muzzle speed that each model of the gun is achieving.

Figure 19 compares the muzzle speed for different reservoir pressures for inviscid and viscous for the numerical case, but also compares experimental results measured with the air gun tested at UC3M facilities, so it allows to analyze how realistic the model of the gas gun designed with LS-Dyna is. Taking a look at the inviscid muzzle speeds, they are smaller for pressures below 3 bar but they

keep on increasing without settling, therefore become higher than for the other cases. On the other hand, the viscous model seems to adequately recreate the actual gas gun, showing not only very similar muzzle speeds but also the same behavior when changing the reservoir pressure.

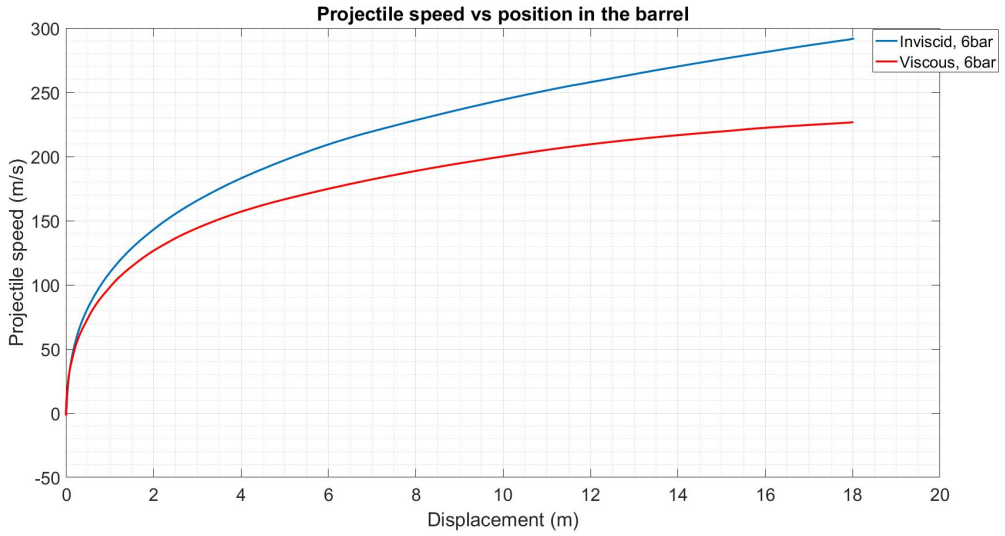

Figure 17: Projectile speed vs position along the barrel for inviscid and viscous flow comparison

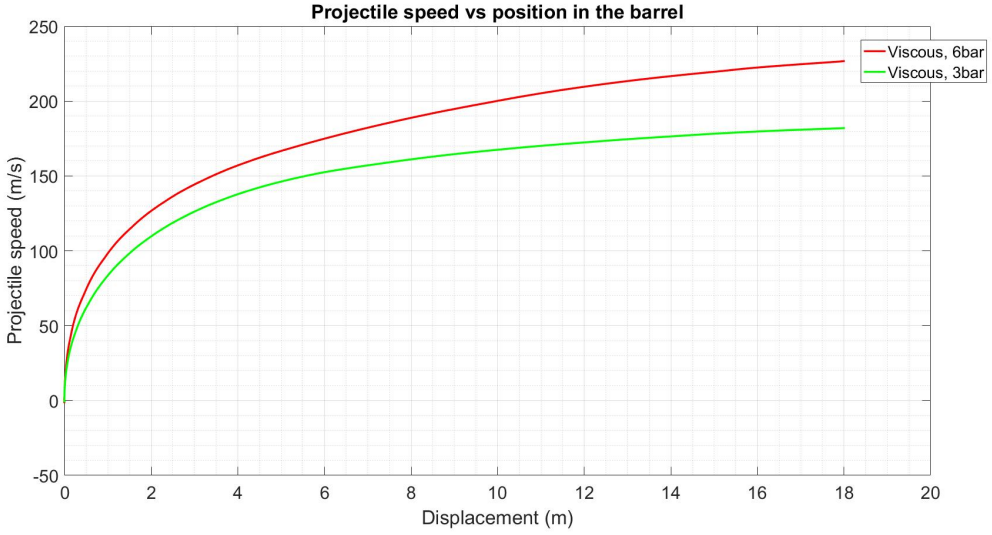

Figure 18: Projectile speed vs position along the barrel for 3bar and 6bar reservoir pressure comparison

Last graph of this section shows the evolution with time of the pressure measured

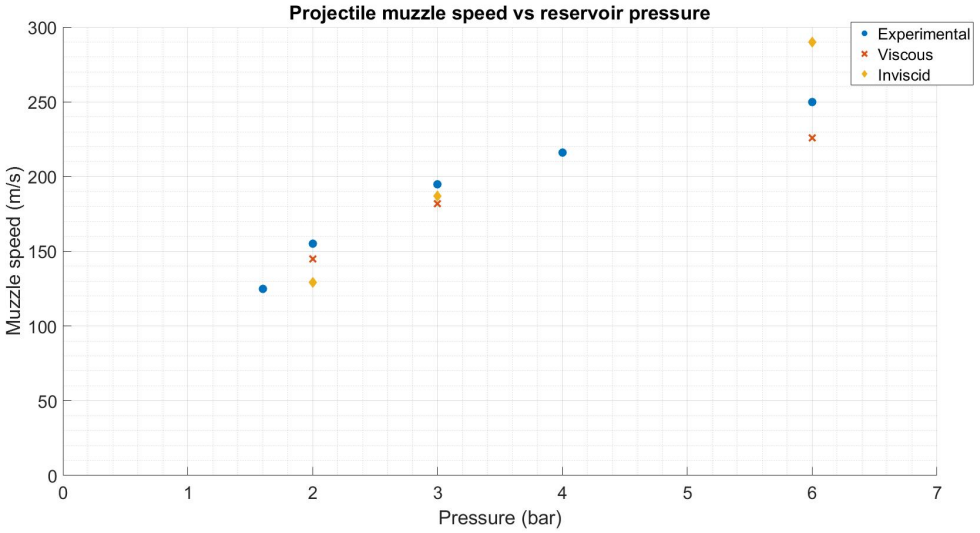

Figure 19: Comparison of experimental and numerical calculated (both viscous and inviscid solution) resultant muzzle speed for different reservoir pressures

at three different nodes of the reservoir. It depicts a nearly linear decrease of the pressure, which at the moment the projectile leaves the barrel, shows a decrease of a 16% with respect to the initial pressure. This result leads to the conclusion that the variation of pressure is not small enough as to model the reservoir as a prescribed boundary so it would act as a pressure inlet, therefore reducing notably the computational times.

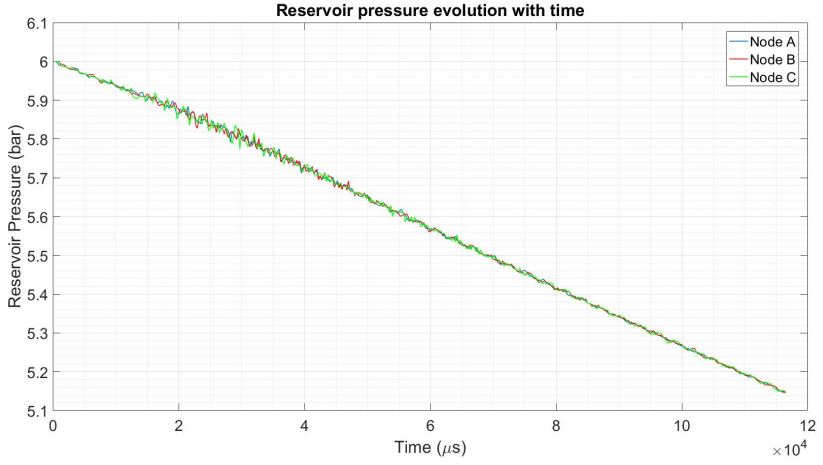

Figure 20: Pressure variation at three different nodes inside the reservoir during the shot

In fact, computational times were incredibly high for these models, taking about

several days to conclude some of them. For instance, the accuracy required to appropriately model bore distances was very difficult to achieved for such a big model, a 18-meter long gun with elements of at least 0.5mm means more than 2 million elements just in the barrel, besides the local refinement of the mesh is not currently working for the CE/SE solver, the reservoir grid elements should be as small as the barrel ones, all of this leads to the conclusion that such model is very difficult to handle with the available tools, in order to achieve the desired accuracy.

Then it was decided to analyze a smaller model, so a finer mesh could allow improved accuracy when modeling some of the features of the gas gun. The solution was to design a ping pong gun, which is much smaller, and both prepare a numerical model to analyze the performance of the gun and built a real ping pong gun to compare the numerical results as described in following sections.

4 Ping pong gun

The ping pong gun is basically a system that makes use of compressed gas to launch ping pong balls, the intention of this section was to design and study the gun but also analyze the feasibility of making it supersonic. To do so, the gun is composed of two tubes, one thick and short which is the pressure reservoir and other longer and thinner which is the barrel, and connecting them, a convergent-divergent nozzle is placed in such a way that the nozzle entry has the same cross sectional area as the reservoir and the nozzle exit has the same cross sectional area as the barrel. During this section, both the numerical models and the experimental prototype will be described. In figure 21 the LS-Dyna model of the supersonic ping pong gun is shown. Keep in mind that the way it works is not only by the high pressure gas in the reservoir but also by making vacuum in the barrel, so there is a seal between this parts, located before the nozzle, that breaks when a determined pressure difference is reached, releasing the gas and propelling the ball.

Notice that the target is to compare the experimental and numerical results, so the numerical model has been designed from the dimensions of the gun that was to be built. The characteristics of the real gun will be described more in detail later on this paper, nevertheless, due to manufacturing issues the dimensions of the prototype were kind of restricted, indeed it was difficult to acquire an appropriate tube for the reservoir. For instance, it was impossible to find a tube with an inner diameter in which the ping pong ball adequately fits, so finally the balls to be used during the tests were made with the 3D printer (the good point is that several projectile masses can be tried depending on the thickness of the printing). On the other hand, the convergent-divergent nozzle has been made by means of a 3D printer, so there is no limitation here about the dimensions and several cases were prepared. The final dimensions of the gun were:

- Propellant gas: Air
- Barrel length: 2.5m
- Caliber: 36.2mm
- Reservoir: 0.008 m^3 at 4 bar

In practice, a ping pong ball would be deformed under the high pressures suffered in the barrel, nevertheless, as own-made PLA balls with better resistance and slightly heavier are to be used, it can be considered to keep its shape during the shot, therefore maintaining constant its aerodynamic performance.

Figure 21: Ping pong gun axisymmetric model

4.1 Numerical models

4.1.1 Control case

First, a control case has been computed in order to understand the performance of the ping pong gun so it can be modified and optimize. This case has the dimensions previously determined for the gun and the dimensions for the nozzle are 6cm long for both convergent and divergent part with a throat radius of 1 cm. Figure 22 depicts the evolution of the ping pong ball speed as it travels through the barrel of the gun. Differently from the 18-meter gun described in previous section, although the evolution describes similar behavior, the initial increase in the speed is not as sharp as before, nevertheless, it keeps on increasing through all the barrel in a way such that from 1 to 2 meters, the speed is increased 50 m/s, so now it would be favorable to slightly increase the length of the gun.

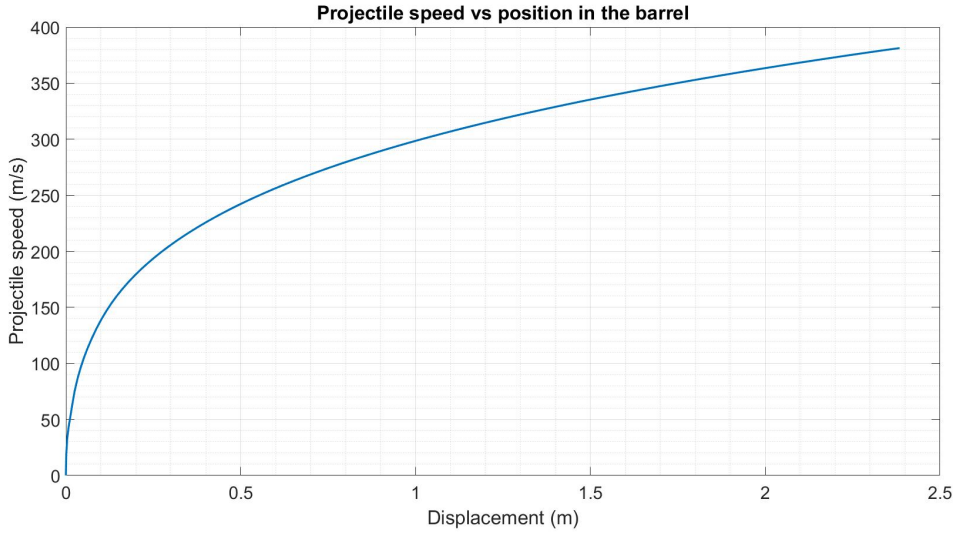

Figure 22: Projectile speed vs position along the barrel for the Ping pong gun control case

As it was done previously, the vorticity at the barrel entry and around the projectile has been studied. Figure 23 shows that although there is some vorticity appearing in the nozzle right after the seal breaks and the gas is released, it almost completely disappear from the nozzle, so the incoming flow from the reservoir is

smoothly introduced in the barrel. It will be seen later when analyzing the nozzle lengths that if the nozzle is too short, vorticity appears in the throat as it becomes narrow.

About the vorticity around the ball, it is also present as expected from previous models, but now its effect is slightly increased as there exists some bore distance (0.5 mm) which allows some flow to overcome the ball and generating some vorticity in the front.

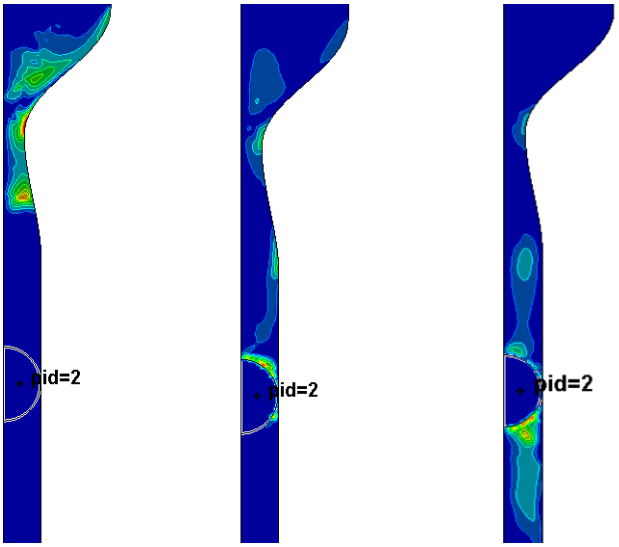

Figure 23: Vorticity at the nozzle and around the projectile during the shot

Finally for this control case, it was decided to plot the velocity, temperature, pressure and Mach number of the flow at different points of the nozzle, to say, the nozzle entry, the throat and the exit. Again, these quantities have been measured at nodes located at the symmetry axis.

Figure 24 shows the evolution of the flow velocity with time at the three points. It can be seen that for the first instants when the seal breaks and the gas is released there is a high peak present in the three curves, this is due to the fact that as the high pressure gas is released, it discharges into vacuum, so there is a notable discontinuity and the flow has to be adapted to the low pressure. This phenomenon is clearly appreciated in figure 26, it can be seen how at the nozzle entry the initial pressure is 4 bar (the reservoir pressure) but as the seal breaks, the pressure starts decreasing to the barrel pressure, but as the jump is so shark, a shock wave is required to increase the pressure and to adapt the flow. These graphs also depict the choking of the convergent part. Velocity, temperature and pressure are nearly constant at the entry and throat of the nozzle, as the pressure difference is enough to choke the flow so at the convergent part the velocity can

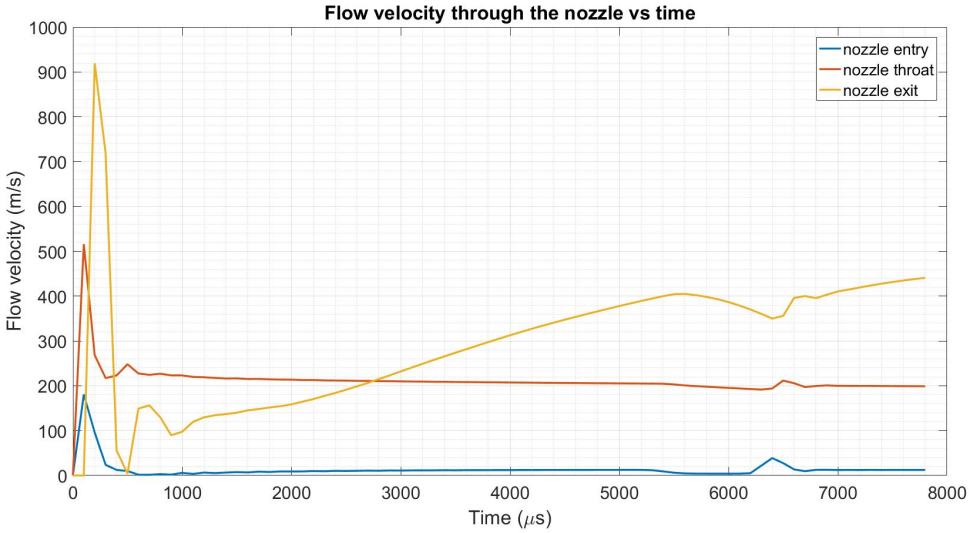

Figure 24: Flow velocity measured at the symmetry axis at the nozzle entry, throat and exit for the control case at different time-steps

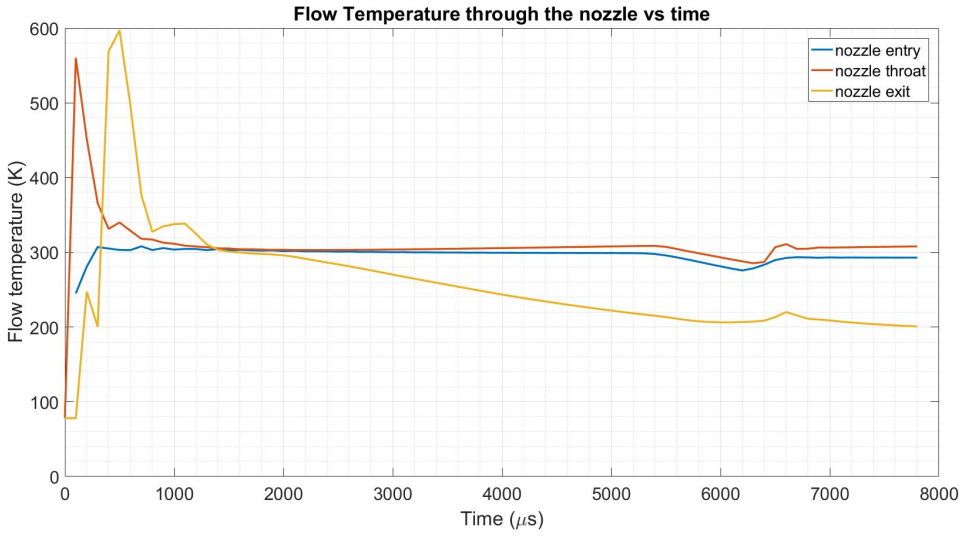

Figure 25: Flow temperature measured at the symmetry axis at the nozzle entry, throat and exit for the control case at different time-steps

not further increase. On the other hand, it is shown that for the divergent part, as the flow develops a supersonic expansion, the velocity keeps on increasing while the pressure decreases, this is consistent with the theory explained in section 1.3.2 of this paper about the nozzle flows.

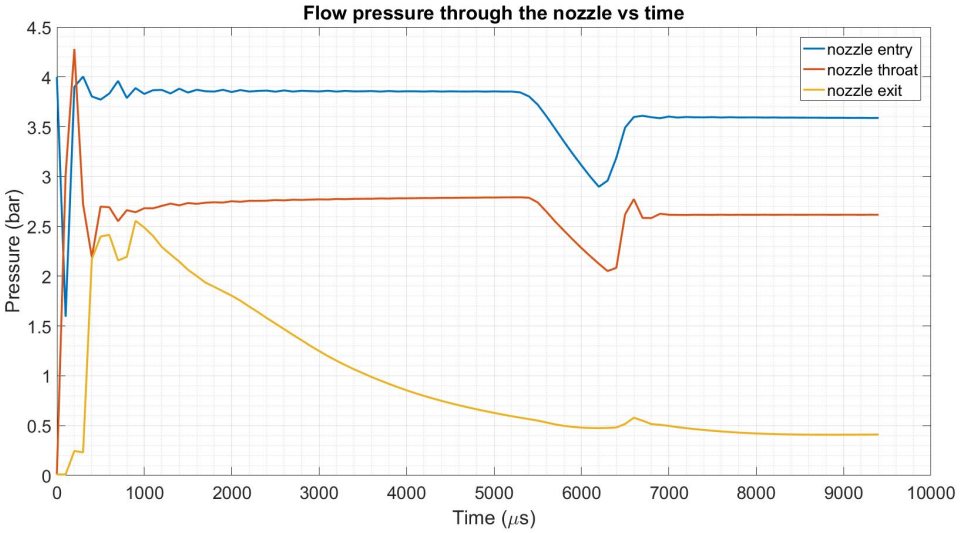

Figure 26: Flow pressure measured at the symmetry axis at the nozzle entry, throat and exit for the control case at different time-steps

When looking to the Mach number evolution in figure 27, it can be seen that at the entry the Mach number is very small, this is due to the fact that the entry is next to the reservoir where the gas is stagnant and its velocity is almost zero. About the Mach number at the exit, it clearly goes supersonic as the reservoir discharges into the barrel, this result is very important as it shows the capability of LS-Dyna CE/SE solver in solving convergent-divergent nozzle and supersonic flows. Finally, when looking at the Mach number at the throat of the nozzle, it is not 1 as theory says but just 0.6, this is because in the numerical simulation the sonic conditions reached not exactly at the throat but a little bit afterwards in the divergent section, so there is a point at the beginning of the divergent section where the flow reaches sonic conditions and the Mach number is kept constant and equal to 1 for any time, downstream this point, the Mach number evolution would describe a curve similar to the one at the throttle exit in figure 27.

Figure 28 and figure 29 show the Mach number evolution with time measured at the node where sonic conditions are reached and the location of the node within the nozzle respectively. So for the nodes of the nozzle downstream this point, the flow quantities are not limited and for instance, the Mach number will increase to values greater than one.

To continue, several models will be proposed and studied for the ping pong gun, so different nozzle dimensions, projectile masses, reservoir pressures and more features are to be analyzed in the following.

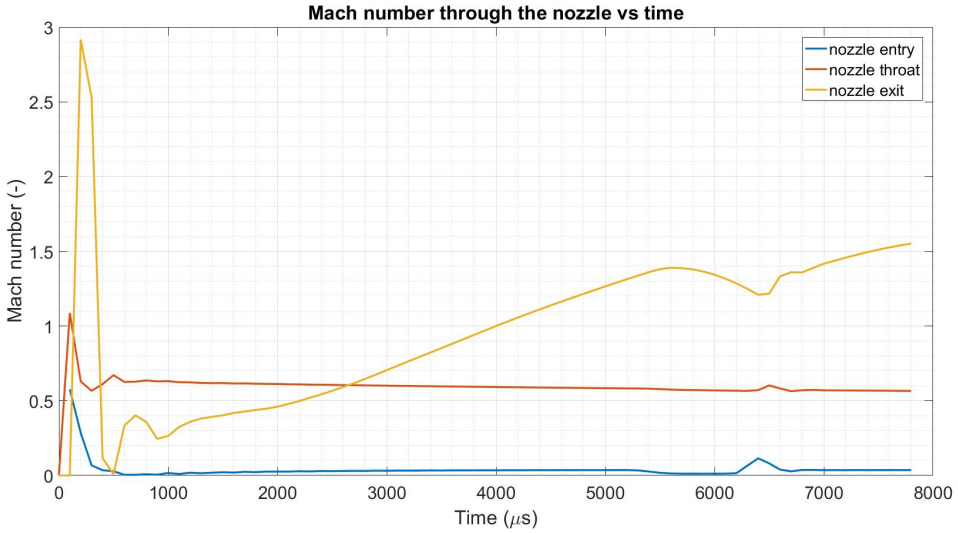

Figure 27: Mach number evolution with time at the nozzle entry, throat and exit for the control case

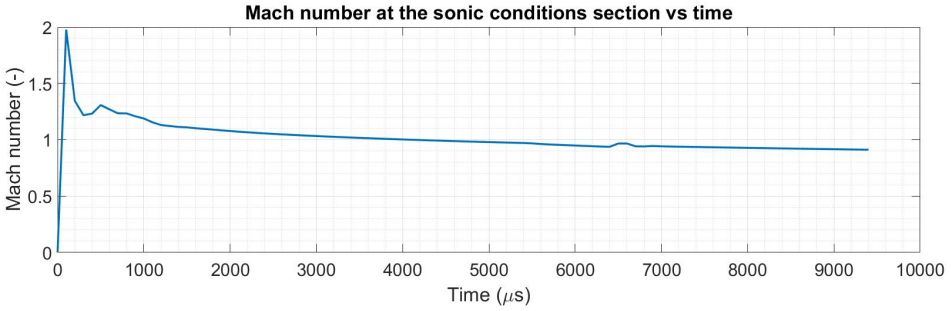

Figure 28: Mach number evolution with time at sonic conditions section for the control case

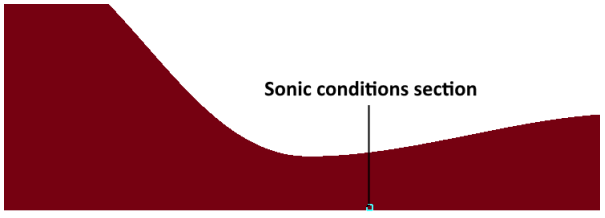

Figure 29: Node where sonic conditions are reached

4.1.2 Nozzle length

Let's start with the study of the longitude of the convergent-divergent nozzle implemented in the supersonic gun for a pressure of 4 bar in the reservoir. First

picture shows the projectile speed evolution along the longitudinal coordinate of the barrel for different nozzle lengths such that the length of the convergent part is the same as for the divergent. It can be seen that although the variation of the speed is very similar for the different lengths, the muzzle speed seems to increase as the nozzle length is decreased up to a point, about 6 cm, when the muzzle speed suddenly decreases, this would be the minimum longitude of the nozzle. Figure 31 shows the vorticity appearing for the case of 2 cm long nozzle. As the throat of the nozzle is extremely narrow, it generates a vorticity which blocks the outgoing flow from the reservoir, this is why there exist a minimum nozzle length related with the cross sectional area of the nozzle inlet.

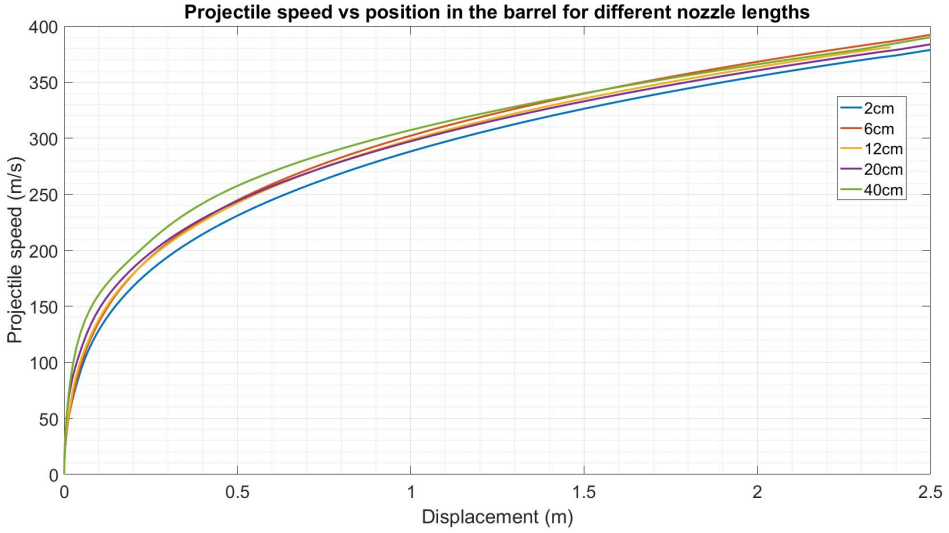

Figure 30: Projectile speed vs position along the barrel for different nozzle lengths 4 bar reservoir pressure

Figure 31: Vorticity appearing at too short nozzles

4.1.3 Nozzle throat area

Now, keeping constant a length of 12 cm for the nozzle, the throat cross sectional area has been changed in order to study the impact of this dimension not only on the muzzle speed but also on the Mach number and the mass flow rate.

Looking at the projectile speed evolution in the barrel, the behavior again is similar for the different cases, except from the nozzle with convergent part only which depicts a more sharpened increase at the first centimeters of the barrel. Regarding the muzzle speeds, the variation in the muzzle speed is notable now, with an increment of about 100 m/s between the case with 1 cm radius nozzle throat and the one which is only convergent.

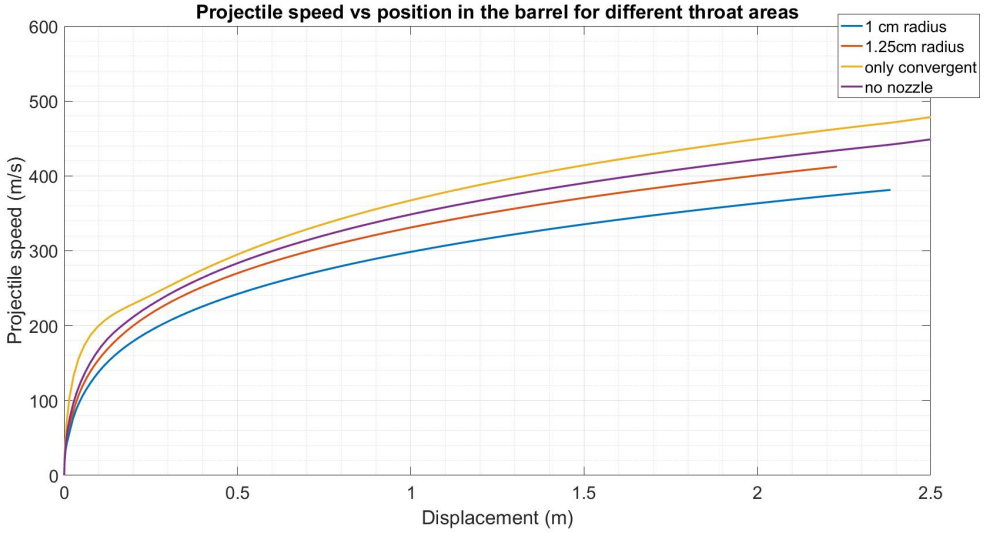

Figure 32: Projectile speed vs position along the barrel for different throat radius, only convergent nozzle and without any nozzle

In order to understand these results, the Mach number and the mass flow rate at the nozzle have been plotted for the cases of 1.25 cm radius nozzle throat and the only convergent nozzle, so the results can be compared with the control case shown in figure 27. Here, it can be seen in figure 34 that the mass flow at the nozzle entry, throat and exit is almost the same being consistent with the mass conservation (the difference is due to numerical issues) with a value about 0.6 kg/s, which is smaller than the 0.8 kg/s of average show in figure 35 for the only convergent nozzle, this would explain why the muzzle speed is slightly higher for the case with only convergent nozzle. When looking at the Mach number evolution with time, for the case of 1.25 cm radius nozzle throat, the results are very similar to the ones obtained for the control case (recall the control case is 1

cm radius nozzle throat), the Mach near the reservoir is close to zero, at the throat is slightly smaller than one for the same reason as before, the sonic conditions are slightly displaced to the divergent part, and at the exit the Mach number keeps on increasing until reaching 1.4 at the moment the projectiles leaves the barrel. Differently, figure 35 shows that the Mach number at the barrel entry is close to one (it is exactly equal to 1 at some point slightly downwards the throat similarly to previous cases for the C-D nozzle throat) but apart from some peak due to numerical issues, it never becomes greater than one, meaning that the flow is not getting supersonic in this case, as deduced from equation 9 of the theory.

Figure 33: Mach number evolution with time at the nozzle entry, throat and exit for 1.25cm radius nozzle throat

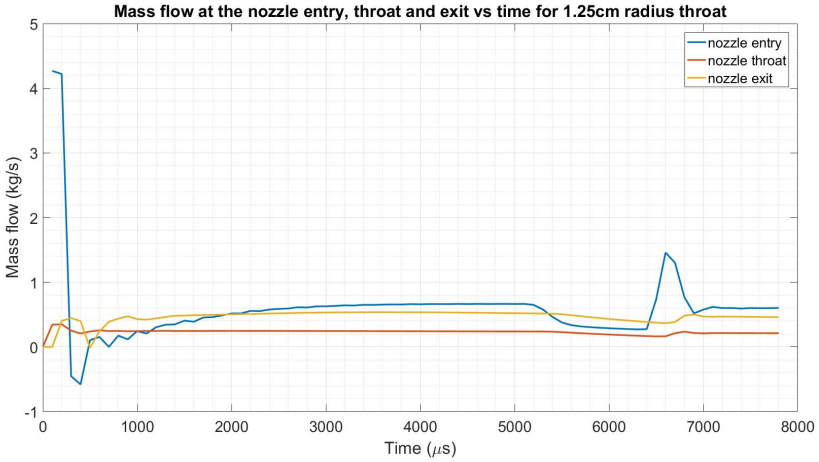

Figure 34: Mass flow evolution with time at the nozzle entry, throat and exit for 1.25cm radius nozzle throat

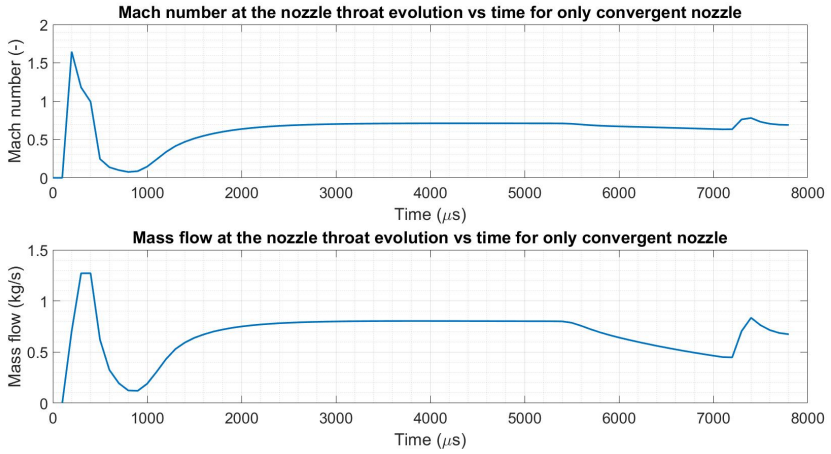

Figure 35: Mach number and mass flow evolution with time at the nozzle entry, throat and exit for only convergent nozzle

4.1.4 Projectile mass

In order to study the launching capabilities of the gun, the control model (4 bar, 1 cm radius nozzle throat) has been calculated with different projectile masses, so the evolution of the muzzle speed with the projectile mass can be obtained. Notice that the muzzle speed decreases exponentially as the launched mass is increased, obviously if the reservoir pressure and the shape of the projectile are kept constant, when the mass is increased the speed is decreased as deduced from equation 17.

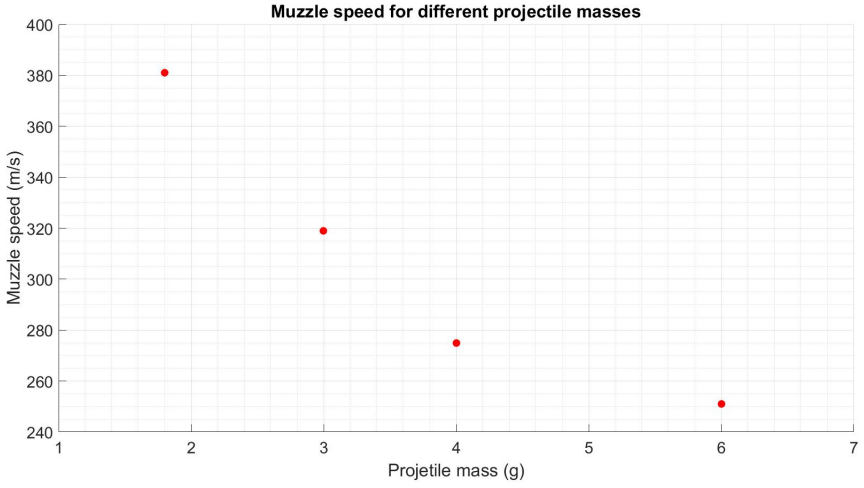

Figure 36: Projectile speed at the muzzle for different projectile masses

$$F = ma = PS \quad \rightarrow \quad \frac{dv}{dt} = \frac{PS}{m} \tag{17}$$

4.1.5 Reservoir pressure

Now, instead of changing the projectile mass, the reservoir pressure is going to vary for the control case and for the 1.25 cm radius nozzle throat so the impact on the muzzle speed can be measured. Figure 37 compares the muzzle speed evolution for the two cases. The behavior seems to be quite the same, approaching an asymptote for the muzzle speed at 10 bars, nevertheless, the 1 cm radius case settles around 500 m/s speed whilst the 1.25 cm radius case does it slightly higher, at 550 m/s, an expected result from previous section comparing the dimensions of the nozzle.

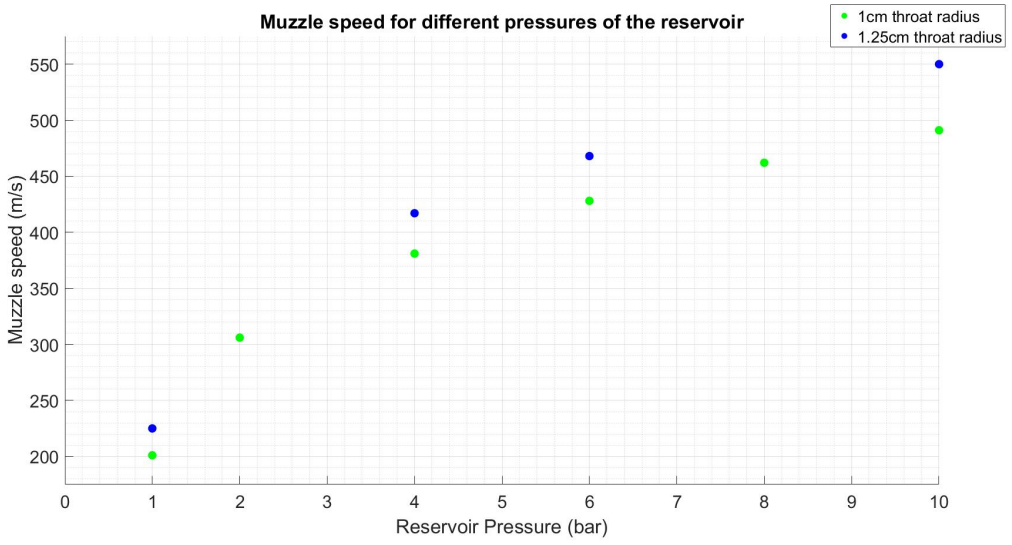

Figure 37: Projectile speed at the muzzle for different reservoir pressures

In order to explain these results, the Mach number of the flow together with the mass flow rate at the nozzle exit, of the 1 cm and 1.25 cm radius nozzle throat cases, have been plotted for different reservoir pressures as shown in figures 38 and 39. Looking first at the Mach number, it can be seen that there is a peak due to the pressurized gas discharge into the vacuum but after the flow adapts, the growth of the Mach is smooth, similar thing happens with the mass flow rate. For the two cases the mass flow rate settles at the first time steps of the shot for the different pressures, nevertheless, for the 1.25 cm radius case, this quantity is slightly higher, leading to the greater muzzle speeds obtained with this case.

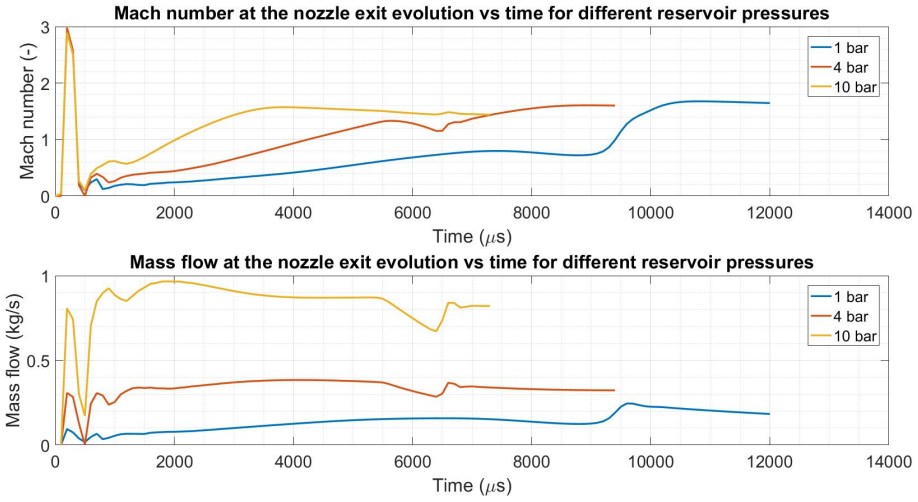

Figure 38: Mach number and mass flow evolution with time at the nozzle exit for different reservoir pressures

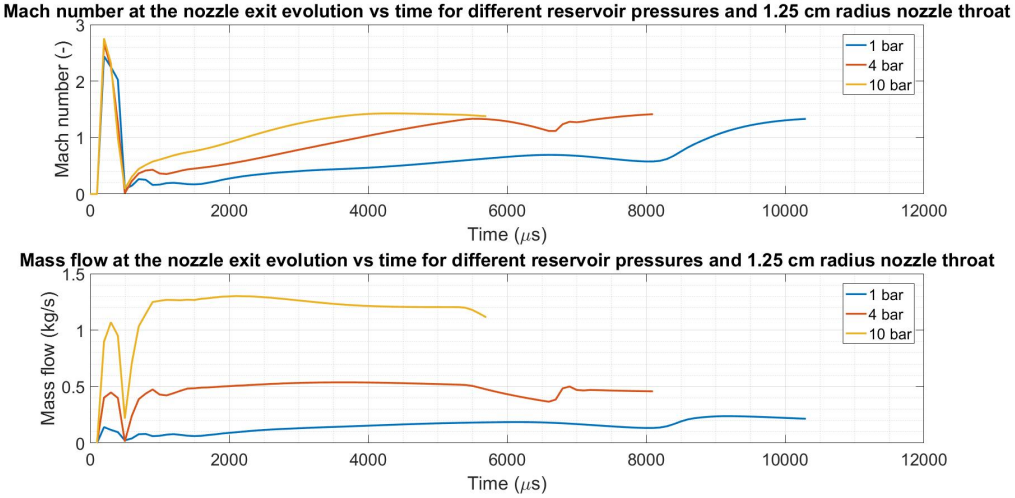

Figure 39: Mach number and mass flow evolution with time at the nozzle exit for different reservoir pressures and 1.25 cm radius nozzle throat

By this time, the reader may have notice the wide variety of parameters that are involved in this problem, nozzle length, nozzle areas, reservoir pressures, etc. The purpose of this paper is to study the impact of the main parameters on the muzzle speed. With further development, it would be interesting to create a map relating nozzle lengths, throat areas and reservoir pressures with muzzle speed, nevertheless the computational issues of this work are very costly and would take long time.

4.1.6 Bore distance

Another important parameter in the model is the bore distance, recall that it is the difference between the radius of the projectile, in this case the ball and the inner radius of the barrel. In practice it must be selected in such a way that there exist no friction between the projectile and the barrel but if it is too wide, there would be high pressure losses which are detrimental for the speed of the projectile. To study the impact of the bore distance on the muzzle speed, the projectile radius has been modified in the control case so different bores have been calculated keeping constant the mass of the projectile. These results are shown in figure 40, which shows that in a range from 0.5 to 1.5 mm of bore distance, the resulting muzzle speed is quite the same, meaning this is a good bore distance for this model, if the bore would be greater than this, there would be too much flow overpassing the projectile therefore reducing notably the pressure at its back and reducing the speed that it can reach.

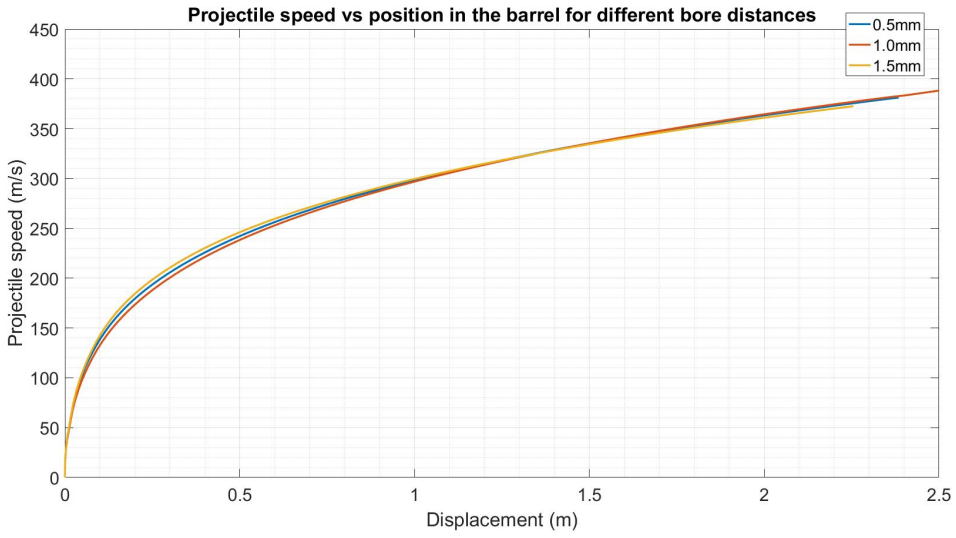

Figure 40: Projectile speed vs position along the barrel for different bore distances

The pressure in the reservoir is probably the most affected quantity by selection of one bore distance or another due to the pressure losses mentioned before. Considering this, the pressure evolution with time has been tracked for several points of the reservoir so the average pressure has been plotted for the three different bore distance cases analyzed as shown in figure 41. It can be seen that although the reduction in reservoir pressure is very small, the case with the smallest bore distance counts with higher reservoir pressure the most of the time as deduced before.

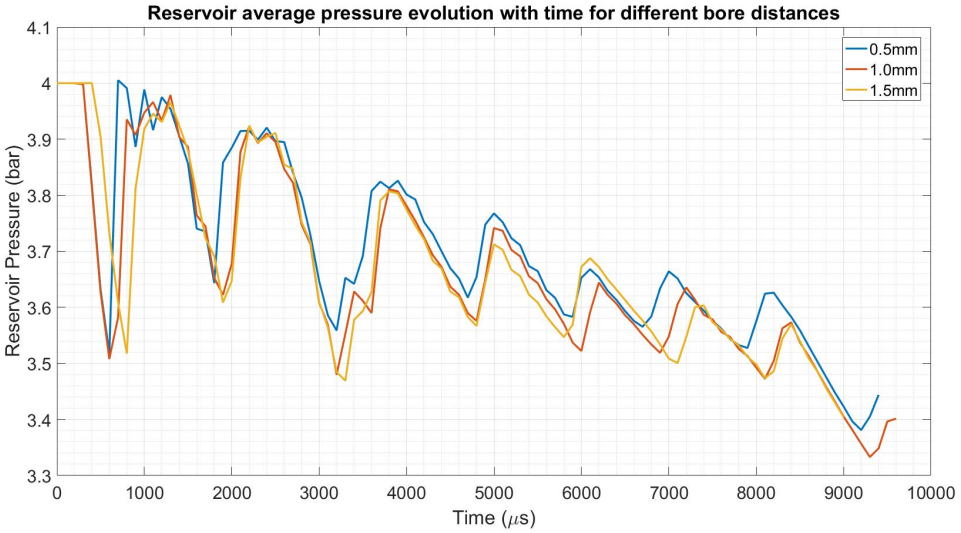

Figure 41: Average reservoir pressure evolution with time for different bore distances

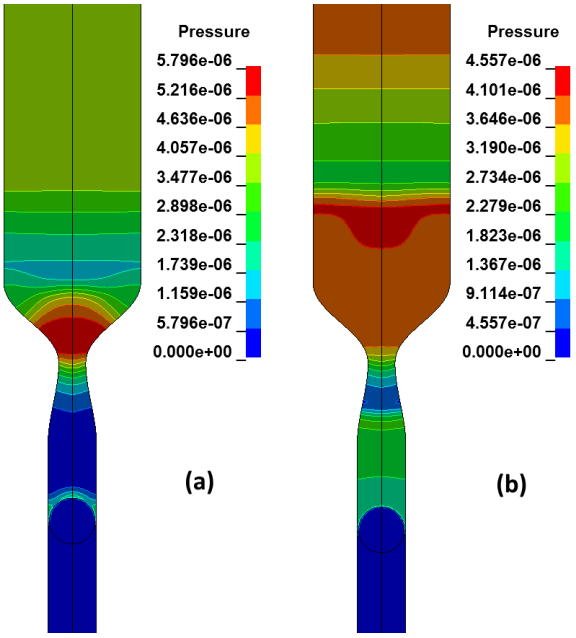

Figure 42: Shock propagation at the reservoir after breaking the seal. $t = 200\mu s$ (a), $t = 500\mu s$ (b). Pressure in bar times 10^{-6}

Here it can be seen that the pressure decrease in the reservoir during the shot is not smooth as it was for the 18 m gun (figure 20), the evolution for the ping pong gun shows peaks which are due to the normal shock wave, created when the

seal separating high pressure air and vacuum collapses, which propagates through the reservoir from left to right several times. Figure 42 shows the normal shock generated before the nozzle, where the seal is located, propagating towards the reservoir. Notice that the simulation was still axisymmetric but the visualization has been reflected to better observe the phenomena represented.

4.1.7 No vacuum inside the barrel

One of the main features of the proposed ping pong gun is the vacuum made inside the barrel, as it allows the ball to be propelled without suffering any deceleration due to air friction within the gun. Just to see the impact of having a 99.9% vacuum in the barrel, figure 43 shows the projectile speed evolution of the projectile with vacuum compared to a case where there is air at ambient conditions in the barrel instead of vacuum.

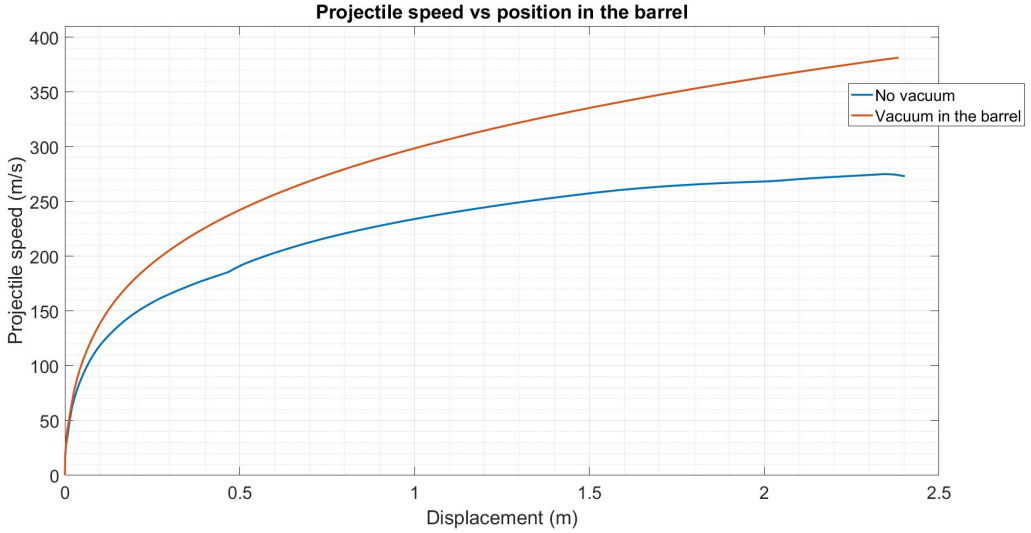

Figure 43: Comparison of projectile speed vs position along the barrel for control case and no vacuum in the barrel case

4.1.8 Propellant gas: Helium

To finish with the ping pong gun, the control case has been computed once again (with 4 bar reservoir pressure) but this time, the propellant gas is Helium instead of air. One can deduce that if the speeds previously obtained are of the order of 400 or 500 m/s, the convergent-divergent nozzle would not be needed for helium as its corresponding sound speed is about 1000 m/s, so the reservoir exit would not get choked for the range of pressures of this analysis, nevertheless,

an isentropic subsonic flow would be expected to be developed through the nozzle.

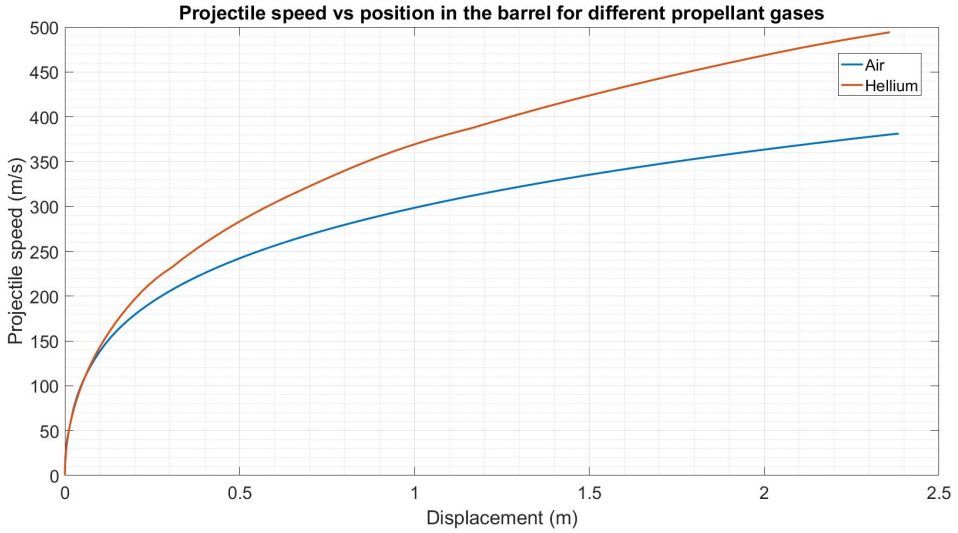

Figure 44: Comparison of projectile speed vs position along the barrel for helium as propellant gas

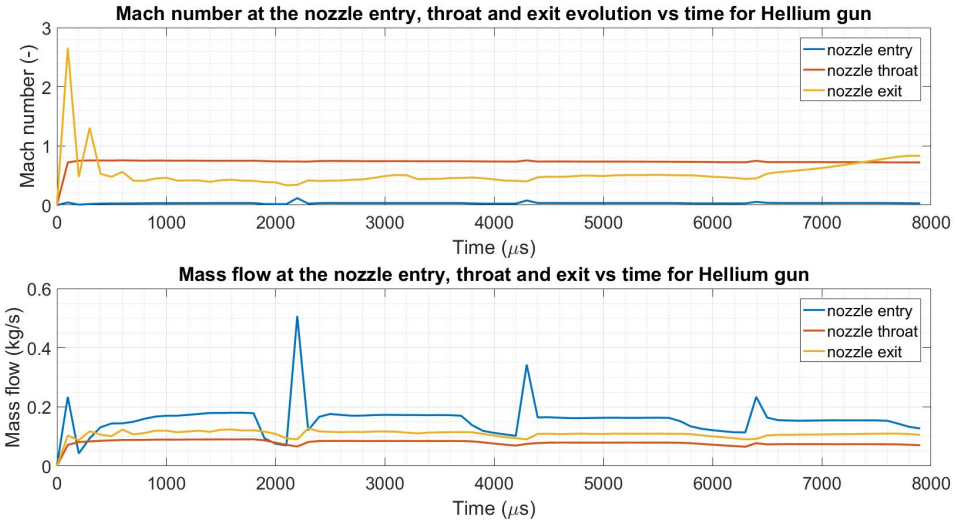

Figure 45: Mach number and mass flow evolution with time at the nozzle entry, throat and exit for helium as propellant gas

Figure 44 compares the projectile speed obtained with helium and air as propellant gases, showing the better performance and efficiency of the helium (light gas) for this application. Figure 45 shows the Mach number and mass flow rate measured at the nozzle entry, throat and exit of the gun powered by helium. It can be seen here that the Mach number is smaller than 1 during the shot, meaning that sonic conditions have not been reached for this pressure, indeed, the maximum Mach number is obtained at the throat, as it is characteristic from the isentropic subsonic flow through a convergent-divergent nozzle explained in the theory. Recall that although the Mach number is smaller than one at the nozzle exit, the flow accelerates in the constant area section until reaching sonic conditions (sonic conditions are reached for long enough tube as explained in section 1.3.3) which for helium means 3 times faster flow than for air when the flow is choked, which explains the higher muzzle speed obtained with helium.

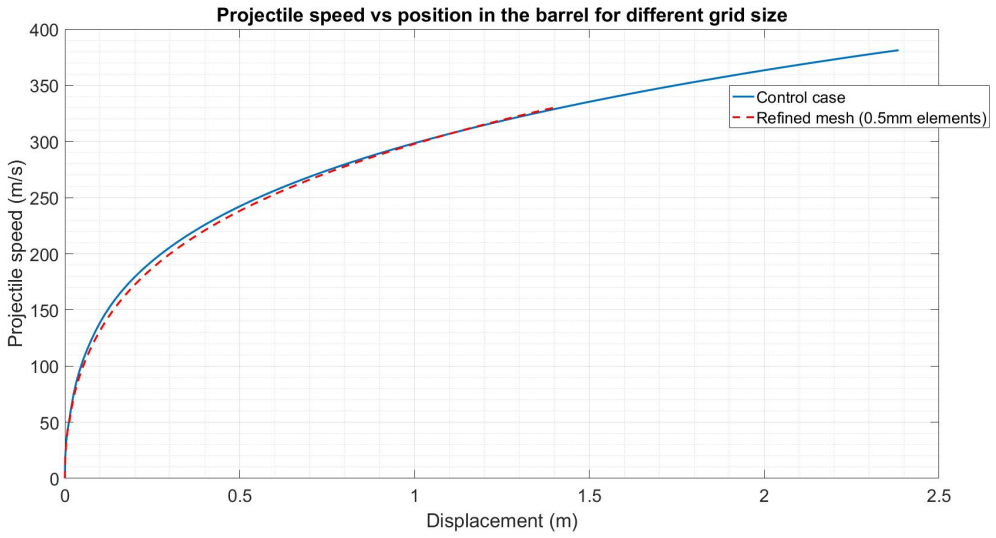

Figure 46: Projectile speed comparison between the control case (1 mm size elements) and the finer mesh case (0.5 mm size elements).

4.1.9 Mesh refinement

In order to check the validity of the results and the convergence of the solution, a finer grid has been implemented in the ping pong gun to check the accuracy of the mesh used during this project. The element size of the control case is 1 mm (recall that these are square elements) whilst the finer mesh is composed by elements of 0.5 mm, half the size of the previous one, in other words, 180000 elements. Keep in mind that for this finer grid the computational times are incredibly high, about one week to simulate the whole shot, so due to technical issues, figure 46 shows the projectile speed evolution up to 1.5 m in the barrel instead of the whole gun,

compared with the control case, which is enough to conclude that the error between them is minimum and for the scope of this project, this small error makes up with reduced computational times and more handleable models.

4.1.10 Projectile free flight

In addition to the models devoted to the analysis of the gun performance, a simple model was built to study the behavior of the ping pong ball leaving the gun flying at supersonic speed in ambient room conditions. It was expected that the air resistance which was avoided in the barrel by creating vacuum inside now will rapidly decelerate the ball. Notice that for this model, the air which flows after the ball when it leaves the barrel has been neglected so the only effect taken into account is the ambient air.

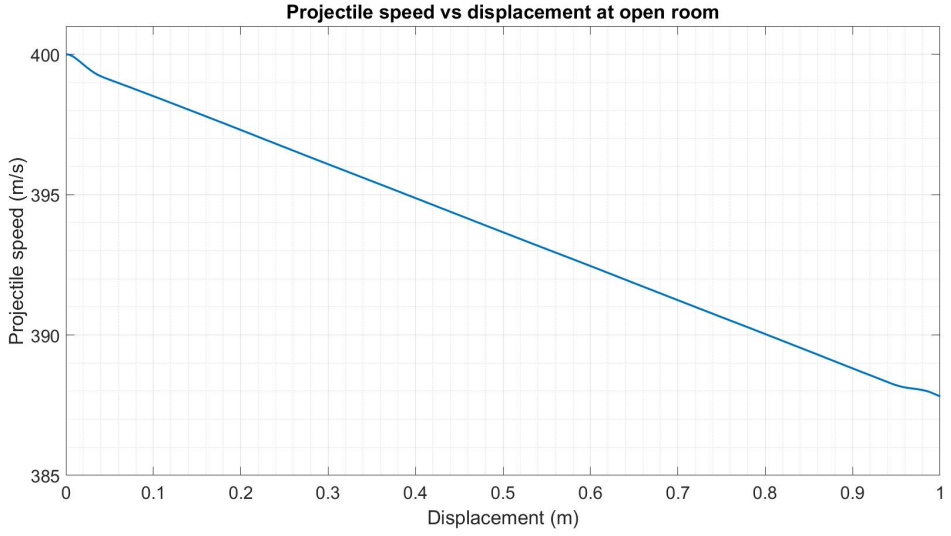

Figure 47: Projectile speed decrease on free flight after living the barrel at 400m/s

Figure 47 shows that when the ball has traveled 1 meter after leaving the barrel, its speed has been linearly reduced from 400 m/s to 385 m/s, which in fact is not very bad for technical purposes. Imagine that the projectile to be used has a complex shape or is not rigid, so during the shot while inside the barrel it is placed within a sabot which is separated after leaving the barrel. These sabots are designed in such a way that they required a small distance to separate from the projectile just by means of the air resistance but without perturbing the trajectory of the projectile, this means that the target which receives the impact must be placed at a minimum distance so it is not hit by the sabot but only by the projectile. Therefore, it is important that after this minimum distance,

the projectile has not seen its speed notably reduced. Just as a curiosity, figure 48 shows the oblique shock wave appearing at the front of the ball moving to the right supersonically modeled with LS-Dyna shock wave detection capabilities.

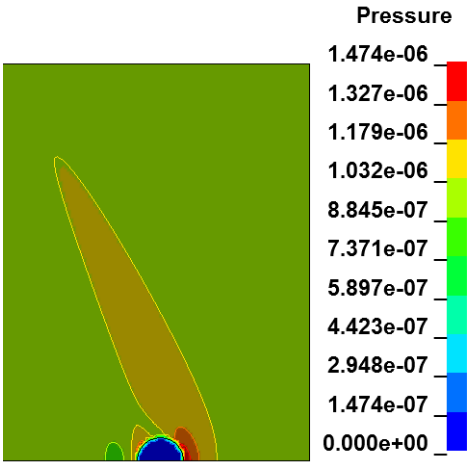

Figure 48: Shockwaves appearing at the nose of the ping pong ball flying at supersonic speed (pressure in bar times 10^{-6})

4.2 Experimental Ping pong gun

As it was previously mentioned, a prototype for the supersonic ping pong gun has been designed and built, although it is still receiving modifications. During this section, the different parts composing the gun are to be described.

Figure 49: Ping pong gun rendered model

The ping pong gun is basically composed by two PVC tubes which can withstand up to 10 bars of internal pressure, allowing the safe working of the gun for the

range of reservoir pressure of 4 or 6 bar as used during this paper. The thicker tube which acts as the gas reservoir has an inner diameter of 101.6 mm, a wall thickness of 4.2 mm and a longitude of 1 meter. The barrel has an inner diameter of 36.2 mm with a wall thickness of 1.9 mm and 2.5-meter length. Notice that these dimensions where selected for convenience of both performance but also manufacturing of the gun.

At one end of the reservoir, it is placed a solid cap which has been 3D printed of PLA (polylactic acid), it has been designed with tow holes where the adapters for the air compressor hose and the barometer are placed and sealed.

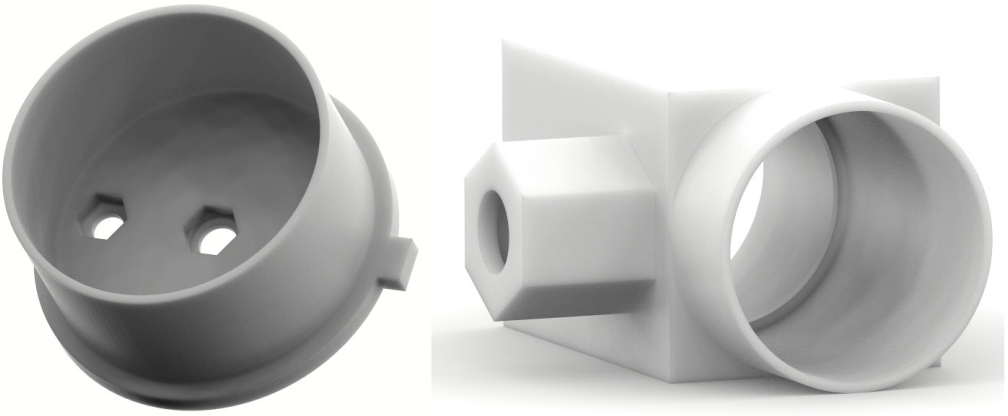

Figure 50: Left: Reservoir cap. Right: Muzzle part

Connecting the reservoir and the barrel of the gun it is placed the most complex part of the system, the 3D printed nozzle. Initially, the convergent-divergent nozzle was designed in such a way that it was introduced by one side into the barrel and by the other side to the reservoir. Keep in mind that a seal made of duct tape or similar material has to be placed at the nozzle entry, so the part has to be designed in such a way that the nozzle can be removable so it allows to put a new seal for each shot and if desired, use other nozzle with different dimensions. The key point was how to make this part removable avoiding any leakage in the reservoir. The solution was to combine the nozzle with an external thread as shown in figure 51. Notice that there is a gap between the convergent section and the thread with the sideboards, the reservoir is introduced in this gap with the seal already located at its end. Then another part shown in figure 52 with an internal threading which rounds the reservoir is screwed in the external thread of the nozzle so it tights up the sideboards against a rubber seal placed in the outer wall of the reservoir and sealing the high pressure gas.

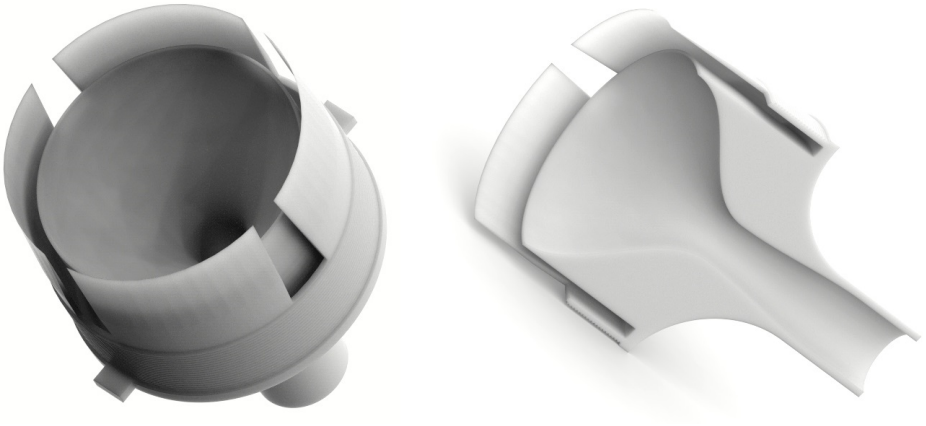

Figure 51: Left: Convergent divergent nozzle with threading. Right: Section view of the convergent-divergent nozzle.

Figure 52: Threading adjustment

Finally, at the muzzle of the barrel, another 3D printed part is located. This part shown in figure 50 right, is designed so an adapter for the vacuum pump can be placed and sealed at one side of the component. Then, duct tape is placed at the front of this part to keep the vacuum inside the barrel. Notice that when the pressure difference between reservoir and barrel is enough to brake the seal, the gas is released so it propels the ball through the barrel, nevertheless, as some gas flows between the ball and the barrel inner wall, this gas reaches the front of the barrel, taking out the duct tape slightly before the ball reaches the muzzle so the duct tape does not affect the ball leaving the gun.

Due to printing time of the components and other practical issues, the gun was not finalized by the moment this paper is written, but it is still being modified to be working as soon as possible.

5 Conclusion and further work

Throughout this paper, several aspects of gas guns have been analyzed both theoretically and numerically in order to have a better understanding of what happens inside the gas gun. During the modeling of the gun, several issues were encountered. The global dimensions of the 18 meters long air gun of the university's facilities revealed to be very complicated to handle, as the large grid required to appropriately solve the discharge of the gas and the flow in the barrel around the projectile increased the numerical calculations to the limits, as a consequence, the computational time was largely increased. Nevertheless, when modeling and solving for the exact launching test, as performed with the university's air gun shooting 140 grams projectiles, the results appeared to be very accurate and the muzzle speeds obtained were very close to the experimental results. This showed that the implementation of the reservoir and barrel shapes, the opening valve and the cylindrical sabot, together with the pressurized gas, high speed flows and FSI (Fluid Solid Interaction) were suitably modeled with LS-Dyna and solved with the new CE/SE solver.

Regarding the study of the ping pong gas gun, the different features of the gun were fathomed. For this model, different reservoir pressures and projectile masses were simulated in order to develop a shooting curve that could be later used in the experimental prototype. The most important part of the analysis of this gun was the convergent-divergent nozzle to be implemented, which allows the flow inside gun to reach supersonic speeds. Regarding the nozzle, different lengths, cross-sectional areas and shapes were calculated so the impact of this parameters on the behavior of the gun could be understood in order to improve the prototype. Indeed, this calculations were used to select the minimal length of the nozzle and the most optimal nozzle throat to exit area ratio for the range of pressures at which the prototype would function. In addition, the flow quantities as, velocity, flux impulse, mass flow or Mach number, were also tracked in the numerical calculations so that, from a fluid dynamics approach, the response of the gun could be interpreted and understand what was happening with the flow, which in the end, is the responsible of reaching one muzzle speed or another.

Summarizing, the results from numerical calculations were very satisfactory in terms of fulfilling the objective of this project. On the other hand, it must be noticed that there are still some deviations in some of the results. For example when tracking the flow Mach number, it was seen that for the supersonic cases, the sonic conditions were reached slightly downstream the throat section. This may be due to the characterizing of the grid, which on the contrary, appeared to be precise enough and the solution converged for the projectile speed evolution. Nevertheless, with further development and resources, an improved grid could be implemented to reach more accurate results.

Regarding the experimental prototype, it was an idea that came up during the project, as it would be interesting to compare the numerical results with test results performed in the laboratory. Although the materials needed are relatively cheap, the complexity of the nozzle made by 3D printing and the shooting system to be implemented, delayed the development of the gun, however, it is expected to have an operative prototype very soon.

A Economic framework

The approximate budget for the realization of this project has been gathered in the next table:

Total engineer hours (h)	600	
Engineer cost/hour (€/h)	35	
		21000 €
LS-Dyna Licence (1 year)	2500 €	
Matlab Licence (1 year)	8.000 €	
		10500 €
PVC tubes	25 €	
Vacuum pump	60 €	
Compressor hoses	20 €	
PLA filament (3kg)	60 €	
Miscellaneous	30 €	
		215 €
	TOTAL	31715 €

B Reduced input

This appendix shows the .k file which runs LS-Dyna. In particular, this reduced input belongs to the ping pong gun model, but keep in mind that the cards used for the UC3M gun model are exactly the same, the only difference is on the values of several parameters as temperature, pressure or heat capacities and the dimensions of the grid, shown in segment, element and node cards, for which only the first lines has been put here, recall that each node and element require a line for its definition.

```
$# LS-DYNA Keyword file created by LS-PrePost(R) V4.3.14 - 16Aug2017
$# Created on Sep-09-2017 (17:24:27) by Alfredo Escalante
*KEYWORD
*PARAMETER
$# Units in (g/mus/cm)
$#   prmr1      val1     prmr2      val2     prmr3      val3     prmr4      val4
R    t_end12000
R  dt_plot100
R dt_fluid0.00005
Rcfl_fluid0.5
R t_1     250
R p_1     1e-8
R t_2     300
R p_2     4e-6
R cv      717.5e-8
R cp      1004.5e-8
R w       130
*TITLE
$#                                                                         title
LS-DYNA keyword deck by LS-PrePost
*CONTROL_ENERGY
$#    hgen      rwen    slnten     rylen
         2         2         2         2
*CONTROL_HOURGLASS
$#     ihq        qh
         1       0.1
$
$--- Fluid
$
*CONTROL_TERMINATION
$   endtim    endcyc     dtmin     endeng   endmas
$#  endtim    endcyc     dtmin    endeng    endmas
&t_end             0       0.0       0.01.000000E8
*CONTROL_TIMESTEP
$#  dtinit    tssfac      isdo    tslimt     dt2ms      lctm     erode     ms1st
1.00000E-4       0.7         0       0.0       0.0         0         0         0
$#  dt2msf   dt2mslc     imscl    unused    unused     rmscl
       0.0         0         0                           0.0
*DATABASE_ELOUT
$#      dt    binary      lcur     ioopt   option1   option2   option3   option4
       1.0         1         0         1         0         0         0         0
*DATABASE_GLSTAT
$#      dt    binary      lcur     ioopt
       1.0         1         0         1
*DATABASE_MATSUM
$#      dt    binary      lcur     ioopt
       1.0         1         0         1
*DATABASE_NODOUT
$#      dt    binary      lcur     ioopt   option1   option2
       1.0         1         0         1       0.0         0
*DATABASE_SLEOUT
$#      dt    binary      lcur     ioopt
```

```
       1.0         1         0         1
*DATABASE_SSSTAT
$#      dt    binary      lcur     ioopt
       1.0         1         0         1
*DATABASE_BINARY_D3PLOT
$#      dt      lcdt      beam     npltc    psetid
&dt_plot           0         0         0         0
$#   ioopt
         0
*DATABASE_EXTENT_BINARY
$#   neiph     neips    maxint    strflg    sigflg    epsflg    rltflg    engflg
         0         0         3         0         1         1         1         1
$#  cmpflg    ieverp    beamip     dcomp      shge     stssz    n3thdt   ialemat
         0         0         0         1         1         1         2         1
$# nintsld   pkp_sen      sclp     hydro     msscl     therm    intout    nodout
         0         0       1.0         0         0         0
$#    dtdt    resplt     neipb
         0         0         0
*SECTION_SHELL
$#   secid    elform      shrf       nip     propt   qr/irid     icomp     setyp
         2        14       1.0         2       1.0         0         0         1
$#      t1        t2        t3        t4      nloc     marea      idof    edgset
       0.0       0.0       0.0       0.0       0.0       0.0       0.0         0
*MAT_RIGID
$#     mid        ro         e        pr         n    couple         m     alias
         7      0.08       2.5       0.3       0.0       0.0       0.0
$#     cmo      con1      con2
       0.0         0         0
$#lco or a1        a2        a3        v1        v2        v3
       0.0       0.0       0.0       0.0       0.0       0.0
*PART
$#                                                                         title
LSHELL2
$#     pid     secid       mid     eosid      hgid      grav    adpopt      tmid
         2         2         7         0         0         0         0         0
*SET_SEGMENT
$#     sid       da1       da2       da3       da4    solver
         1       0.0       0.0       0.0       0.0CESE
$#      n1        n2        n3        n4        a1        a2        a3        a4
     25220         1         1         1       0.0       0.0       0.0       0.0
     32515         2         2         2       0.0       0.0       0.0       0.0
         2     32507     32507     32507       0.0       0.0       0.0       0.0
     25352         4         4         4       0.0       0.0       0.0       0.0
...

*SET_SEGMENT
$#     sid       da1       da2       da3       da4    solver
         2       0.0       0.0       0.0       0.0CESE
$#      n1        n2        n3        n4        a1        a2        a3        a4
     25327       502       502       502       0.0       0.0       0.0       0.0
      1752     25322     25322     25322       0.0       0.0       0.0       0.0
      1753     25344     25344     25344       0.0       0.0       0.0       0.0
...

*SET_SEGMENT
$#     sid       da1       da2       da3       da4    solver
         3       0.0       0.0       0.0       0.0CESE
$#      n1        n2        n3        n4        a1        a2        a3        a4
         1     25217     25217     25217       0.0       0.0       0.0       0.0
     25325      1752      1752      1752       0.0       0.0       0.0       0.0
      1761     32279     32279     32279       0.0       0.0       0.0       0.0
      1762     25325     25325     25325       0.0       0.0       0.0       0.0
...

*ELEMENT_SOLID
$#   eid     pid      n1      n2      n3      n4      n5      n6      n7      n8
       1       1       1   25217   25221   25220   25220   25220   25220   25220
       2       1    3544   25222   25226   25225   25225   25225   25225   25225
       3       1    3543   25227   25230   25229   25229   25229   25229   25229
```

```
       4       1    3520   25231   25234   25218   25218   25218   25218   25218
       5       1    3521   25235   25238   25232   25232   25232   25232   25232
       6       1    3522   25239   25242   25236   25236   25236   25236   25236
       7       1    3523   25243   25246   25240   25240   25240   25240   25240
...

*NODE
$#   nid               x               y               z      tc      rc
       1             0.0          -100.0             0.0       0       0
       2             0.0             0.0             0.0       0       0
       3             0.0           -99.8             0.0       0       0
       4             0.0       -99.60001             0.0       0       0
       5             0.0       -99.40001             0.0       0       0
...

*CESE_INITIAL
$#       u         v         w       rho         p         t
                                                &P_1      &T_1
*CESE_INITIAL_SET
$    setID      Duic       vic       wic     rhoic       pic       tic
         1                                              &P_2      &T_2
*CESE_CONTROL_SOLVER
$   iframe     iflow     igeom
$#   icese     iflow     igeom    iframe
       200         1       101         0
*CESE_CONTROL_TIMESTEP
$     iddt       cfl     dtint
$#    iddt       cfl     dtint
         2&cfl_fluid&dt_fluid
*CESE_CONTROL_LIMITER
$    idlmt      alfa      beta      epsr
$#   idlmt      alfa     beta       epsr
         0       0.0       1.0       0.5
*CESE_BOUNDARY_AXISYMMETRIC_SET
$#    ssid
         1
*CESE_BOUNDARY_NON_REFLECTIVE_SET
$#    ssid
         2
*CESE_BOUNDARY_SOLID_WALL_SET
$#    ssid      lcid        vx        vy        vz
         3         0       0.0       0.0       0.0
*CESE_PART
$      pid       mid     eosid
$#     pid       mid     eosid
         1         6         3
*CESE_EOS_IDEAL_GAS
$    eosid        cv        cp
$#   eosid        cv        cp
         3&cv       &cp
*CESE_MAT_GAS
$#     mid        c1        c2        pr
         61.4580E-11     110.4      0.72
*END
```

C Gantt diagram

Next figure represents the Gantt diagram of the project:

ACTIVITY	ID	Starts (month)	Ends (month)
Research	1	1	9
LS-Dyna models	2	1	3
UC3M gun model	3	4	8
Ping pong gun model	4	9	12
Ping pong gun prototype	5	9	12
Report	6	10	12

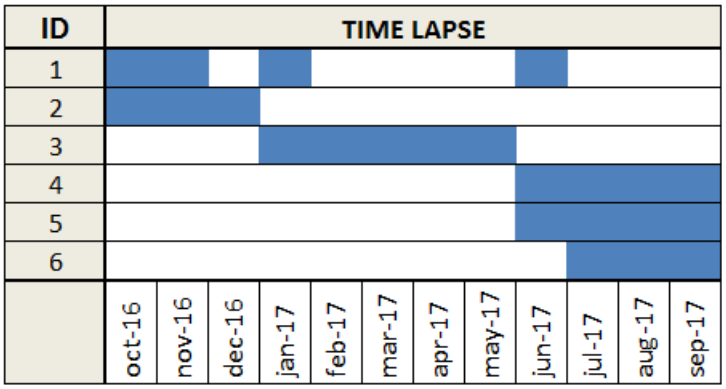

Figure 53: Project Gantt diagram

References

[1] Patrick Ky, "SESAR and the environment", Brussels, 2010.

[2] A320 Aircraft family, 2017, taken from www.aircraft.airbus.com/aircraftfamilies/passengeraircraft/a320family/a320neo/

[3] Angel Arias, Jorge Lopez-Puente, Jose Antonio Loya, David Varas and Ramon Zaera, Department of Continuum Mechanics and Structural Analysis, University Carlos III of Madrid, Spain "Analysis of high-speed impact problems in the aircraft industry", 2014.

[4] A. Grimaldi, A. Solloa, M. Gudab, and F. Marulob. "Parametric study of a SPH high velocity impact analysis. A bird strike windshield application. Composite Structures", 2013.

[5] Horizon 2020, The EU Framework Programme for Research and Innovation, taken from ec.europa.eu/programmes/horizon2020/

[6] S.A. Meguid, R.H. Mao, and T.Y. Ng. "FE analysis of geometry effects of an artificial bird striking an aeroengine fan blade". International Journal of Impact Engineering, 2008

[7] R. Budgey. "The development of a substitute artificial bird by the international birdstrike research group for use in aircraft component testing". In International Bird Strike Committee, Amsterdam, The Netherlands, 2000.

[8] Pernas Snchez, Jess, "Anlisis y simulacin de impactos de hielo sobre laminados carbono/epoxi", Madrid, 2013.

[9] Artero Guerrero, Jos Alfonso, "Anlisis y modelizacin del golpe hidrodinmico en tanques integrados de combustible realizados en material compuesto", Madrid, 2014.

[10] NASA Remote Hypervelocity Test Laboratory, NASA, taken from www.nasa.gov/centers/wstf/laboratories/hypervelocity

[11] Hallock F. Swift, "High-Pressure Shock Compression of Solids VIII, Chapter 1, Light-Gas Gun Technology: A Historical Perspective", Berlin, Germany, 2005.

[12] THIOT Ingenierie. www.thiot-ingenierie.com

[13] H. W. Liepmann and A. Roshko, "Elements of Gasdynamics", New York, USA, 1957.

[14] John D. Anderson, Jr, "Fundamentals of aerodynamics", New York, USA, 2011.

[15] Shapiro, A.H., "The dynamics and thermodynamics of compressible fluid flow, Volume 1", Ronald Press, USA, 1953.

[16] Space-Time Conservation Element Solution Element Method, 2006, NASA, taken from www.grc.nasa.gov/WWW/microbus/

[17] Livermore Software Technology (LSTC), "LS-DYNA Keyword user manual Volume III"